METHODOLOGIES FOR TRANSIENT SIMULATION OF HYBRID ELECTROMAGNETIC/CIRCUIT SYSTEMS WITH MULTIPLE TIME SCALES

BY

ANAND RAMACHANDRAN

B.S., Duke University, 2001
M.S., University of Illinois at Urbana-Champaign, 2005

DISSERTATION

Submitted in partial fulfillment of the requirements
for the degree of Doctor of Philosophy in Electrical and Computer Engineering
in the Graduate College of the
University of Illinois at Urbana-Champaign, 2009

Urbana, Illinois

Doctoral Committee:

Professor Andreas C. Cangellaris, Chair
Professor Umberto Ravaioli
Professor Jose E. Schutt-Aine
Professor Martin D. F. Wong

ABSTRACT

This work presents methodologies to facilitate the efficient cosimulation of electromagnetic/circuit systems while exploiting the multiple time scales that are often present in the numerical simulation of such systems. Three distinct approaches are presented to expedite such a simulation process, with the common theme that the methodologies should allow for the ability to utilize different timesteps in the simulation procedure for the different components appearing in a hybrid system.

The first contribution involves a direct representation of each of Maxwell's curl equations in terms of SPICE-equivalent circuit stamps. This provides for a full-wave, circuit-compatible description of a distributed structure that can very naturally be incorporated into a circuit simulation environment. This capability can be applied to circuit simulations of distributed structures, or it can facilitate the detailed simulation of an electrically small structure with full electromagnetic accuracy.

The second contribution allows for the utilization of different numerical integration schemes and timesteps in the simulation of hybrid structures via a domain decomposition approach. By introducing a novel scheme to combine finite-difference time-domain simulation with SPICE-like circuit simulation, it is shown that the timestep used in the lumped circuit portions need not be limited by the Courant-Friedrichs-Lewy (CFL) limit which governs the timestep used in distributed portions. Additionally, the use of the Crank-Nicolson integration scheme is investigated for the simulation of transmission line structures, and an efficient methodology is proposed by combining the Crank-Nicolson integration of transmission lines and standard integration of circuits.

Finally, the third contribution in this work involves efficient simulation of circuits involving multirate signals with widely separated time scales. An efficient representation of multirate signals is found by introducing a different time variable for each time scale in order to overcome the significant oversampling of such signals that arises from more traditional, univariate representations. This representation is then directly applied to the simulation of transmission line structures. It is found that the resulting methodologies provide for a significant speedup in the overall simulation time.

To my parents

ACKNOWLEDGMENTS

First and foremost, I would like to thank my adviser, Professor Andreas C. Cangellaris, for his patience and dedication in directing my research. Our many conversations have inspired me to think critically when approaching challenging research problems in electrical engineering.

I also thank my Ph.D. committee members, Professor Jose E. Schutt-Aine, Professor Umberto Ravaioli, and Professor Martin D. F. Wong, for their insightful comments. My dissertation has been vastly improved as a result of their input.

Very special thanks also go to my brother, Dr. Aravind Ramachandran, who has always been there for me. The countless hours we have spent proposing, contemplating and debating so many thoughts and ideas have truly helped shape the way I think as well as the person I am.

Additionally, I thank my friends and colleagues in the electromagnetics lab, whose company has made my years in graduate school a very fruitful and enjoyable time. A special note of thanks goes out to Dr. Anne Woo, Johannes Russer, and Prasad Sumant for many thought-provoking discussions as well their sincere friendship.

Finally, and most importantly, I thank my family for their love and support in all of my endeavors. I could never have come this far without all of them, and no number of words can express how much I truly appreciate them always being there for me. Thank you.

TABLE OF CONTENTS

CHAPTER 1 INTRODUCTION 1
1.1 Motivation and Objectives 1
1.2 Overview 3

CHAPTER 2 BACKGROUND 5
2.1 Introduction 5
2.2 The Simulation of Electronic Circuits 5
2.3 Transient Simulation of Distributed Structures Using FDTD 14
2.4 Methods for Combining Circuit Simulation and FDTD Simulation 20

CHAPTER 3 SPICE-COMPATIBLE STAMPS FOR THE NUMERICAL SIMULATION OF MAXWELL'S EQUATIONS IN THE TIME DOMAIN 22
3.1 Introduction 22
3.2 Methodology 24
3.3 Numerical Demonstration 26

CHAPTER 4 A DECOMPOSITION METHOD FOR THE SIMULATION OF HYBRID ELECTROMAGNETIC/CIRCUIT SYSTEMS WITH MULTIPLE TIME SCALES 32
4.1 Introduction 32
4.2 Substitution Theorem from Network Theory 33
4.3 Waveform Relaxation 35
4.4 Methodology 35
4.5 Simulation Studies 37
4.6 Unconditionally Stable Simulation of Transmission Lines 46
4.7 Concluding Remarks 54

CHAPTER 5 THE ANALYSIS OF DISTRIBUTED CIRCUITS WITH WIDELY SEPARATED TIME SCALES USING MULTIVARIATE PDE METHODS 56
5.1 Introduction 56
5.2 Multivariate Representation of Multirate Signals 57
5.3 The Multitime Partial Differential Equation (MPDE) 59
5.4 Time Domain Solution to the MPDE 70
5.5 Application to Transmission Line Circuits 74
5.6 Comments and Conclusions 85

CHAPTER 6 CONCLUSION AND FUTURE WORK 87
6.1 Overview and Impact of Results 87
6.2 Future Work 89

REFERENCES 90

AUTHOR'S BIOGRAPHY 94

CHAPTER 1

INTRODUCTION

1.1 Motivation and Objectives

As modern electronic systems in both the commercial and the military arena become increasingly complex, the ability to prototype and simulate such systems before they arrive at the production stage is imperative for keeping costs and production times down. Contemporary designs are beginning to utilize frequencies approaching tens and hundreds of gigahertz, while device and package sizes continue to shrink. Consequently, the lumped circuit approximation no longer suffices, and the need to consider the distributed, electromagnetic contribution becomes critical for the accurate simulation of such systems. Additionally, the need to consider other physical contributions to the system parameters, such as thermal effects, is becoming increasingly important for providing reliable designs. Finally, many different technologies are being utilized within a single package. For example, a typical wireless communication system on a cellular phone may include one or more antennas as well as micro- or nanoelectromechanical system (MEMS or NEMS) devices as well as standard integrated circuitry. Errors in the design cannot be corrected after fabrication in such a complicated system. Therefore, the need for accurate and efficient numerical prototyping of a system involving many different technologies all working in tandem is obvious.

Another characteristic of modern electronic systems is the ubiquity of multiband and broadband subsystems within a single package or module. One problem with such

systems is the appearance of passive intermodulation noise. Passive intermodulation is the unintentional mixing of signals with two closely spaced frequencies, due to nonlinearities appearing in the signal path. Such nonlinearities may be due to a variety of sources including thermal, mechanical, or magnetic effects. Until recently, the level of passive intermodulation noise has not posed a significant threat to the integrity of wireless systems. But the increased push toward lower power levels in mobile devices means that the signal-to-noise ratio is decreasing, and even small levels of noise are now becoming significant. As such, the phenomenon of passive intermodulation has seen a surge in interest recently and is one of the primary motivators for the present work.

To be able to account accurately for effects such as intermodulation noise, it is necessary to be able to perform simulations of systems that evolve dynamically based on several different physical effects. Given the variety of physical effects involved in the spawning of intermodulation in complex systems, the numerical integration of such a system using a single integration scheme and timestep is clearly prohibitive. The need for a more piecewise approach to the simulation problem is patent, where each individual component of the overall system can be numerically integrated using a timestep and an integration scheme that is most appropriate given the physical nature of that component.

This dissertation presents applicable techniques for the time-domain simulation of complex systems involving subsystems of diverse physical natures, varying significantly in both the spatial and time scales. Several numerical techniques are introduced to facilitate the cosimulation of electromagnetic and circuit systems. The approaches allow the numerical integration scheme and timestep to be chosen individually for each

component subsystem, enabling possible solution avenues to the global simulation problem outlined above.

1.2 Overview

The organization of this dissertation is as follows. Chapter 2 gives a brief overview of some background material pertinent to the topics discussed in the subsequent chapters. First, a general description of the standard circuit simulation technique for transient analysis is given. This is followed by a description of the simulation of distributed structures using the finite-difference time-domain (FDTD) method. The chapter concludes with a brief overview of methods for the simulation of hybrid electromagnetic/circuit systems.

Chapter 3 develops a technique for numerically integrating Maxwell's equations in the time domain using a standard circuit simulation tool such as SPICE. This allows an arbitrary electromagnetic structure, discretized on a rectangular grid using Yee cells, to be transformed into an equivalent circuit form. The ability to simulate electromagnetic structures using circuit simulation tools is of paramount importance, as it means that distributed effects can be accounted for using a lumped model. Also, since circuit simulation programs such as SPICE are in such widespread use and are generally considered the standard method of simulation for most electronic systems, having SPICE-compatible descriptions of distributed electromagnetic structures allows for more efficient integration of such structures into the generic framework of the system than would otherwise be possible using traditional field solvers. In the latter case, more postprocessing of the output of the field solver would be necessary in order to be able to

convert the result into a SPICE-compatible form. The example of a rectangular cavity resonator is used to demonstrate the validity of the method proposed in this chapter.

Chapter 4 begins with a discussion of the substitution theorem from classical network analysis, leading to the waveform relaxation algorithm. Then a decomposition method for hybrid electromagnetic/circuit simulation with multiple time scales is introduced and two examples are given demonstrating its use as well as its advantages. After a discussion of some of the limitations of this proposed methodology related to the conditional stability of the standard FDTD scheme, an alternative method is suggested to overcome such stability issues using Crank-Nicolson integration of the electromagnetic portions. Examples are then shown demonstrating the accuracy and efficacy of this method.

Next, an efficient means of simulating transmission line circuits involving signals displaying multirate characteristics is described in Chapter 5. This enables a compact, multivariate representation of signals with widely spaced frequencies and describes a methodology for directly simulating circuits using the multivariate representation of these types of signals. The method is applied to the simulation of an ideal, lossless transmission line as well as to a transmission line consisting of periodically time-varying dielectric.

The final chapter provides some concluding remarks regarding the impact of each of the methodologies described in the previous chapters. It also outlines some further work that is yet to be done in the directions introduced in this dissertation.

CHAPTER 2

BACKGROUND

2.1 Introduction

This chapter reviews some of the background material pertaining to the time-domain analysis of both circuits and electromagnetic structures. The chapter begins with a description of transient circuit simulation, describing different numerical integration schemes and their stability properties, as well as the Newton-Raphson method for the simulation of nonlinear devices. Then the chapter covers electromagnetic simulation using the finite-difference time-domain (FDTD) method, with a focus on one-dimensional wave propagation through the transmission line model. This is followed by a brief outline of some of the existing methodologies for the time-domain simulation of systems involving hybrid electromagnetic/circuit components.

2.2 The Simulation of Electronic Circuits

A circuit is merely a representation of a system of ordinary differential equations (ODEs). Thus, the circuit simulation problem is to describe the dynamical behavior of the system of ODEs in time under some governing constraints such as charge conservation. In the most general setting, these ODEs will be nonlinear.

Standard circuit simulation involves four main steps [1]:

(i) A nodal analysis to describe the circuit topology in terms of a system of ODEs

(ii) A numerical integration scheme that discretizes the ODEs and converts them into a system of nonlinear algebraic equations

(iii) A Newton-based iterative scheme to linearize the nonlinear algebraic equations

(iv) Some iterative scheme to solve the resulting linear system of equations

Most modern circuit simulation tools, e.g., SPICE, utilize each of these steps in one form or another. In this chapter, we briefly discuss steps (ii) and (iii), as they are the most pertinent steps in developing an understanding of some of the issues in play. Step (i) is most commonly approached using a technique known as Modified Nodal Analysis, and we refer the reader to the discussions available in any one of several circuit simulation textbooks [2, 3]. The solution of the linear system in step (iv) is usually achieved by performing a lower-upper (LU) factorization of the coefficient matrix. However, a detailed discussion of this process is beyond the scope of this dissertation and will not be considered in what follows. Throughout, we will focus on the transient behavior of the system.

2.2.1 Numerical integration of electronic circuits

Begin by considering a simple, generic form for the circuit equations,

$$\frac{d\mathbf{x}}{dt} = F\left(\mathbf{x}, t\right), \tag{2.1}$$

where $\mathbf{x}(t)$ represents the vector of unknowns and t represents time. The function F is a general, possibly nonlinear function encapsulating the device models within the circuit as well as the sources in the system. The initial condition for the differential equation in (2.1) is given as $\mathbf{x}(t_0) = \mathbf{x}_0$, with $\mathbf{x}_0$ constant.

Assume that the circuit has been solved up to some time point $t_{n\text{-}1}$, and let the next time point t_n be defined by $t_n = t_{n\text{-}1} + h$, where h refers to the timestep. We need to define how to find the solution $\mathbf{x}(t_n)$ at time t_n. To accomplish this, we can write the solution $\mathbf{x}(t_n)$ by integrating Equation (2.1) as

$$\mathbf{x}(t_n) = \mathbf{x}(t_{n-1}) + \int_{t_{n-1}}^{t_n} F(\mathbf{x}, t)\, dt\,. \tag{2.2}$$

Now, the approximation of the integral appearing on the right-hand side (RHS) of Equation (2.2) is critical to the resulting solution. The three most commonly used approximations of this integral for the purpose of circuit simulation applications are the forward Euler, backward Euler, and trapezoidal approximations, as defined respectively by Equations (2.3a-c) below,

$$\int_{t_{n-1}}^{t_n} F(\mathbf{x}, t)dt \approx F(\mathbf{x}(t_{n-1}), t_{n-1}) \cdot h \tag{2.3a}$$

$$\int_{t_{n-1}}^{t_n} F(\mathbf{x}, t)dt \approx F(\mathbf{x}(t_n), t_n) \cdot h \tag{2.3b}$$

$$\int_{t_{n-1}}^{t_n} F(\mathbf{x}, t)dt \approx \frac{h}{2}\left[F(\mathbf{x}(t_{n-1}), t_{n-1}) + F(\mathbf{x}(t_n), t_n)\right]. \tag{2.3c}$$

Note that these definitions are respectively analogous to the left, right, and midpoint (or trapezoidal) Riemann sum definitions of the same integral. Each one of these integration schemes will now be developed in a little more detail.

Using the forward Euler integration scheme, the result for the value of the unknown $\mathbf{x}(t_n)$ can be written as

$$\mathbf{x}(t_n) = \mathbf{x}(t_{n-1}) + F(\mathbf{x}(t_{n-1}), t_{n-1}) \cdot h\,. \tag{2.4}$$

This defines an *explicit* update of the solution at the current time point based entirely on known values of the solution at previous time points. Alternatively, the update defined by the backward Euler and trapezoidal schemes define *implicit* relations, shown respectively in Equations (2.5) and (2.6) below. This means that the value of the updated solution $\mathbf{x}(t_n)$ is written in terms of unknown values at time t_n,

$$\mathbf{x}(t_n) = \mathbf{x}(t_{n-1}) + F(\mathbf{x}(t_n), t_n) \cdot h \tag{2.5}$$

$$\mathbf{x}(t_n) = \mathbf{x}(t_{n-1}) + \frac{h}{2}\left[F(\mathbf{x}(t_{n-1}), t_{n-1}) + F(\mathbf{x}(t_n), t_n) \right]. \tag{2.6}$$

The trapezoidal integration scheme can be interpreted as a combination of the forward and backward Euler schemes. As such, it has certain properties that make it more appropriate in certain situations, especially those situations involving wave propagation. This will be addressed further at a later point in this dissertation.

2.2.2 Stability analysis

While the update relations in Equations (2.4)-(2.6) for the three integration schemes defined in the previous section seem somewhat similar upon first glance, they vary drastically in their stability properties. To develop the stability analysis of each integration scheme, consider the test equation defined by

$$\frac{d\mathbf{x}}{dt} = \lambda \mathbf{x}, \quad \mathbf{x}(0) = \mathbf{x}_0, \tag{2.7}$$

where λ is an arbitrary complex number. To be consistent with the modeling of a physical problem, assume $\mathrm{Re}\{\lambda\} < 0$, in which case the solution $\mathbf{x}(t)$ tends to 0 as $t \to \infty$.

Now, assuming a constant timestep h, consider the effect of applying each of the update schemes in Equations (2.4)-(2.6) to the test equation above. Applying the forward Euler scheme gives

$$\begin{aligned} \mathbf{x}(t_1) &= (1+\lambda h)\mathbf{x}(t_0) \\ \mathbf{x}(t_2) &= (1+\lambda h)^2 \mathbf{x}(t_0) \\ &\vdots \\ \mathbf{x}(t_k) &= (1+\lambda h)^k \mathbf{x}(t_0) \end{aligned} \quad . \tag{2.8}$$

This progression satisfies the limiting condition $\mathbf{x}(t_k) \to 0$ as $t_k \to \infty$ provided that $|1+\lambda h| < 1$. Assuming that h is real and positive and letting j represent the imaginary unit satisfying $j^2 = -1$, this is equivalent to restricting λh to the interior of a unit circle centered at -1 in the λh-plane, as demonstrated pictorially in Figure 2.1.

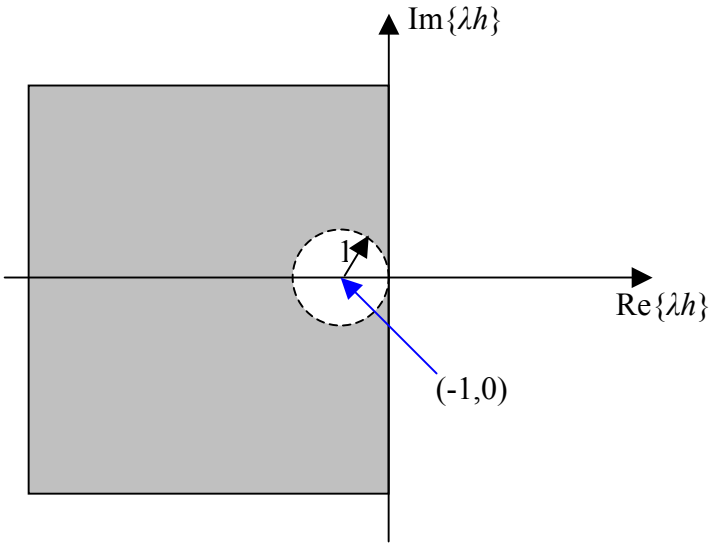

Figure 2.1: Region of convergence for the forward Euler integration scheme.

To understand the significance of the region of convergence for the forward Euler scheme, interpret λ as the eigenvalue of the test equation in (2.7). In other words, λ can

be associated with a characteristic time for the equation, or a measure of how quickly the response of the system approaches 0 as time progresses. As such, the larger the value of λ, the smaller the value of h must be chosen in order to maintain convergence of the numerical integration. Now, for a system which contains both small and large characteristic times, known as a *stiff system*, applying the forward Euler integration scheme necessitates choosing the timestep so as to satisfy the convergence criteria based on the largest eigenvalue of the system, i.e., those poles that decay the fastest. Therefore, the forward Euler scheme is not particularly suitable for the simulation of most classes of circuits and is typically not widely used.

Applying the backward Euler scheme to the test equation in (2.7) gives

$$\begin{aligned} \mathbf{x}(t_1) &= \frac{\mathbf{x}(t_0)}{(1-\lambda h)} \\ \mathbf{x}(t_2) &= \frac{\mathbf{x}(t_0)}{(1-\lambda h)^2} \\ &\vdots \\ \mathbf{x}(t_k) &= \frac{\mathbf{x}(t_0)}{(1-\lambda h)^k} \end{aligned} \quad . \tag{2.9}$$

Convergence of this sequence to 0 is guaranteed if $|1-\lambda h| > 1$, which can equivalently be interpreted as restricting λh to the exterior of a unit circle centered at +1 in the λh-plane. But if we restrict values of λ to satisfy $\mathrm{Re}\{\lambda\} < 0$, then this region of convergence includes the entire left half of the λh-plane. In other words, the backward Euler scheme will converge for any real, positive value of the timestep h. Consequently, the backward Euler scheme is deemed an *unconditionally stable* integration scheme.

Finally, consider the trapezoidal update scheme in Equation (2.6). Applying this scheme to the test equation in (2.7) gives

$$\begin{aligned}
\mathbf{x}(t_1) &= \left[\frac{1+\lambda h/2}{1-\lambda h/2}\right]\mathbf{x}(t_0) \\
\mathbf{x}(t_2) &= \left[\frac{1+\lambda h/2}{1-\lambda h/2}\right]^2\mathbf{x}(t_0) \\
&\vdots \\
\mathbf{x}(t_k) &= \left[\frac{1+\lambda h/2}{1-\lambda h/2}\right]^k\mathbf{x}(t_0)
\end{aligned} \tag{2.10}$$

For the case that $\mathrm{Re}\{\lambda\} < 0$, this progression will satisfy convergence to 0 for any positive real values of *h*. Consequently, the trapezoidal scheme is also unconditionally stable.

2.2.3 Solution of nonlinear equations

In order to be able to solve general, nonlinear device models, it is first necessary to linearize the nonlinear system. This is achieved via the Newton-Raphson method for solving nonlinear equations of the form $f(\mathbf{x}) = 0$.

Consider a nonlinear function $f : \mathbb{R}^n \to \mathbb{R}^n$. The Newton-Raphson method for finding the zeros of *f* proceeds by iteratively constructing local linear approximations to *f* around the solution at the $(k-1)$th iterate in order to define the *k*th iterate:

(i) Begin with an initial guess for the solution, $\mathbf{x}^0$

(ii) At each subsequent iteration *k*, define $\mathbf{x}^k = \mathbf{x}^{k-1} - \left[\mathbf{J}(f)\big|_{\mathbf{x}^{k-1}}\right]^{-1} f\left(\mathbf{x}^{k-1}\right)$, where $\mathbf{J}(f)$ refers to the Jacobian matrix for the function *f*

(iii) If $\|f(\mathbf{x}^k)\| < \varepsilon$ then stop, otherwise return to step (ii); here, ε is some prescribed tolerance and $\|\bullet\|$ is any well-defined norm in $\mathbb{R}^n$

The Newton-Raphson method is normally quite effective for finding solutions to nonlinear equations provided that the initial guess $\mathbf{x}^0$ is reasonable.

Another interpretation of the Newton-Raphson method for the solution of nonlinear device models is to think of each iteration in terms of linearized versions of the models themselves. To illustrate, consider the example of a semiconductor diode element whose *i*-*v* relationship is defined by

$$i_D = I_0\left(e^{v_D/v_{th}} - 1\right). \tag{2.11}$$

In Equation (2.11), I_0 represents the device saturation current (typically on the order of femtoamperes); v_{th} is the thermal voltage, used in the relationship between the electrical current and the electrostatic potential across a p-n junction; and v_D is the voltage across the diode. At a room temperature of 300 K, the thermal voltage is approximately 26 mV.

To linearize the relationship in (2.11), approximate the diode current by a first-order Taylor series about the diode voltage at the *k*th iterate,

$$i_D\left(v_D\right) \approx i_D\left(v_D^k\right) + \frac{\partial i_D}{\partial v_D}\left(v_D^k\right)\left(v_D - v_D^k\right). \tag{2.12}$$

This means that at each iteration of the Newton-Raphson procedure, the diode can be replaced by a parallel combination of an equivalent current source and conductance, as defined by Equations (2.13a-b) and shown in Figure 2.2.

$$G_{eq}^k = \frac{\partial i_D}{\partial v_D}\left(v_D^k\right) = \frac{I_0}{v_{th}} e^{v_D^k/v_{th}} \tag{2.13a}$$

$$I_{eq}^k = i_D\left(v_D^k\right) - G_{eq}^k \cdot v_D^k \tag{2.13b}$$

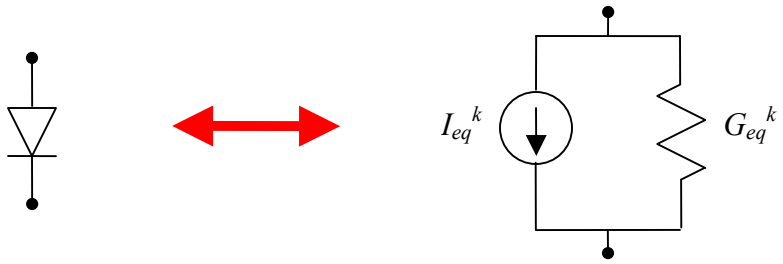

Figure 2.2: Linear equivalent model for the diode.

2.2.4 Some comments about drawbacks of the circuit simulation paradigm

The SPICE model of circuit simulation has been well-developed over the past several decades to handle large, nonlinear circuits based on many of the same principles as those described in the preceding sections. Advanced features such as local truncation error handling via adaptive time-stepping have made SPICE the industry-standard environment for performing circuit design and testing.

However, one of the main drawbacks to the standard SPICE simulation paradigm is that the timestep used in the simulation must be constant throughout the entire circuit. Although unconditionally stable integration schemes are typically used for the numerical time integration, the timestep is still limited by the accuracy requirements. In particular, if one portion of a given circuit is known to respond at a faster rate than other portions, the timestep for the entire circuit must be chosen to satisfy the requirements of the fastest-varying portion of the circuit. As modern designs encompass different subcircuits or subsystems with different physical characteristics, the ability to fully exploit the different scales in characteristic time between the different subsystems will be imperative for efficiently and accurately performing global simulation of hybrid systems.

2.3 Transient Simulation of Distributed Structures Using FDTD

As frequencies increase and switching times shrink, the lumped circuit approximation fails to capture all of the physical effects involved in the dynamic behavior of a system. The insufficiency of the lumped circuit approximation becomes especially apparent for structures that are electrically large. However, the inclusion of simulations with electromagnetic accuracy also becomes critical in the study of localized, detailed effects that cannot be accurately captured by a lumped equivalent circuit. In both of these situations, it becomes necessary to consider the electromagnetic contribution to the system response through the use of full-wave electromagnetic solvers.

Among the various methods used for the transient simulation of the time-varying Maxwell's curl equations, the finite-difference time-domain (FDTD) method has established itself as one of the most popular and widely studied [4]. As a finite method, the FDTD method is based on the direct discretization of the time-varying Maxwell's curl equations appearing in Equations (2.14a-b). The curl operators are approximated using the Yee grid [5] and as such, only local interactions exist between neighboring or nearby locations in the spatial grid. This interaction is defined by a direct enforcement of Maxwell's equations at each grid point, except perhaps at the boundary of the grid, where external conditions may be imposed.

2.3.1 Yee's lattice

To begin, consider the time-varying form of Maxwell's curl equations,

$$\nabla \times \mathbf{E} = -\frac{\partial \mathbf{B}}{\partial t} \tag{2.14a}$$

$$\nabla \times \mathbf{H} = \sigma \mathbf{E} + \frac{\partial \mathbf{D}}{\partial t} + \mathbf{J}^i , \tag{2.14b}$$

where **D** and **B** represent the electric and magnetic flux density vectors, respectively, and $\mathbf{J}^i$ represents any impressed current sources. The flux densities **D** and **B** are related to the electric and magnetic fields via the constitutive relations [6],

$$\mathbf{D} = \varepsilon \mathbf{E}, \ \mathbf{B} = \mu \mathbf{H} . \tag{2.15}$$

For the purpose of the analysis presented here, we will assume homogeneous, isotropic media, implying that ε and μ are scalar and time-invariant quantities. Also, to simplify the analysis, assume that $\sigma = 0$ and that there are no impressed sources in the domain of interest, i.e., $\mathbf{J}^i = 0$. Then, Maxwell's equations can be rewritten in the simplified form

$$\nabla \times \mathbf{E} = -\mu \frac{\partial \mathbf{H}}{\partial t} \tag{2.16a}$$

$$\nabla \times \mathbf{H} = \varepsilon \frac{\partial \mathbf{E}}{\partial t} . \tag{2.16b}$$

In order to discretize the curl operators appearing in Equations (2.16a-b), consider the three-dimensional rectangular Yee's lattice shown in Figure 2.3. According to this lattice, the electric and magnetic fields are defined on a staggered grid, with the electric field variables being defined along the edges of the *primary grid* and the magnetic field variables defined along the edges of the *secondary grid*. Alternatively, the magnetic field can be thought of as being defined through the *faces* of the primary grid. This staggering of the electric and magnetic field variables allows for a natural way to interpret the curl of one field domain around the other.

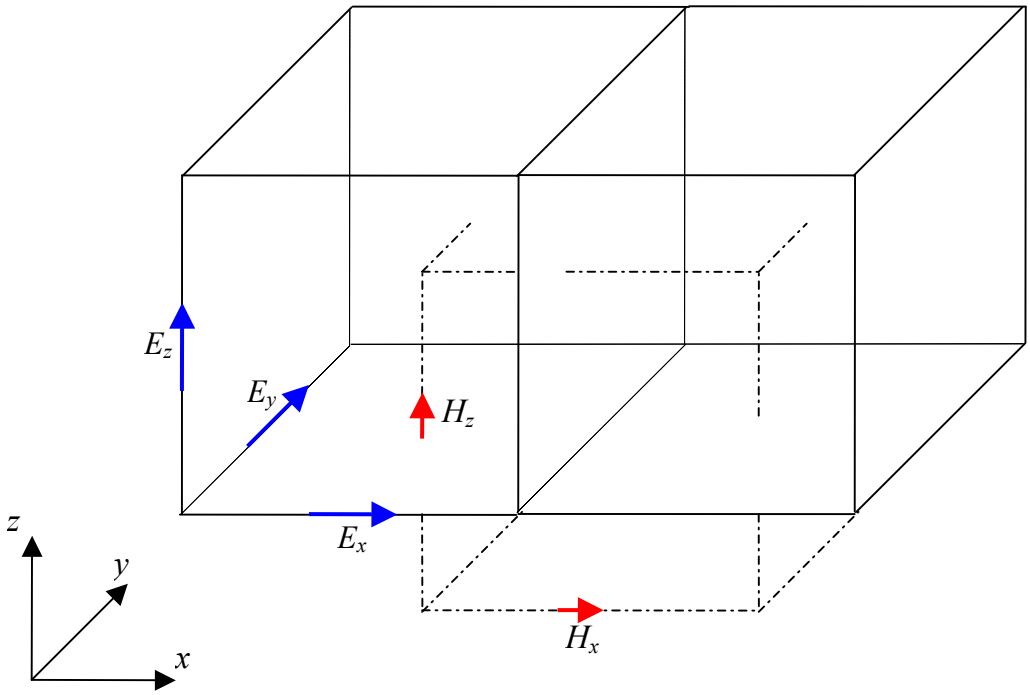

Figure 2.3: Yee's lattice for the discretization of the curl operators. The dark arrows indicate the electric field variables along the edges of the primary grid, while the light arrows indicate the magnetic field variables along the edges of the secondary grid.

In addition to the staggering in space introduced by the Yee grid, the standard FDTD scheme utilizes a staggering in time of one half-step between the electric and magnetic field variables. This allows for an explicit, time-marching scheme, where each of the electric and magnetic field variables is updated using discrete curls computed using previously known field values. This is shown for one dimension each of Faraday's and Ampère's laws below in Equations (2.17a-b), where the spatial location of the field variable (normalized by the grid size in each Cartesian direction) is identified by the triplet appearing in the parentheses, and the temporal location of the field variable (normalized by the timestep) is identified by the superscript:

$$H_z^{p+1/2}\left(i+\frac{1}{2},j+\frac{1}{2},k\right)=H_z^{p-1/2}\left(i+\frac{1}{2},j+\frac{1}{2},k\right)$$
$$-\frac{\Delta t}{\mu\Delta y}\left[E_x^p\left(i+\frac{1}{2},j,k\right)-E_x^p\left(i+\frac{1}{2},j+1,k\right)\right] \quad (2.17a)$$
$$-\frac{\Delta t}{\mu\Delta x}\left[E_y^p\left(i+1,j+\frac{1}{2},k\right)-E_y^p\left(i,j+\frac{1}{2},k\right)\right]$$

$$E_z^{p+1}\left(i,j,k+\frac{1}{2}\right)=E_z^p\left(i,j,k+\frac{1}{2}\right)$$
$$+\frac{\Delta t}{\varepsilon\Delta y}\left[H_x^{p+1/2}\left(i,j-\frac{1}{2},k+\frac{1}{2}\right)-H_x^{p+1/2}\left(i,j+\frac{1}{2},k+\frac{1}{2}\right)\right] \quad (2.17b)$$
$$+\frac{\Delta t}{\varepsilon\Delta x}\left[H_y^{p+1/2}\left(i+\frac{1}{2},j,k+\frac{1}{2}\right)-H_y^{p+1/2}\left(i-\frac{1}{2},j,k+\frac{1}{2}\right)\right]$$

Notice that the update of the electric field variables in Equation (2.17b) uses the latest-known values of the magnetic field at the time point $\left(p+1/2\right)$. The corresponding equations in the other dimensions can similarly be stated in terms of permutations of the Cartesian directions.

2.3.2 Transmission line simulation

To demonstrate a somewhat more concrete application of the standard FDTD method, consider the problem of one-dimensional wave propagation along a transmission line. Wave propagation along more complicated structures such as microstrip lines or other planar lines can be cast in terms of transverse electromagnetic (TEM) wave propagation along the transmission line [7-9]. This means that the transmission line approximation is versatile and useful for modeling many scenarios involving wave propagation.

The voltage and current variables distributed along the transmission line are governed by the *telegrapher's equations*, shown for the lossless case in Equations (2.18a-b) below,

where L_{pul} and C_{pul} represent the per-unit-length (p.u.l.) inductance and capacitance of the line, respectively [10],

$$\frac{\partial V}{\partial z} = -L_{pul}\frac{\partial I}{\partial t} \tag{2.18a}$$

$$\frac{\partial I}{\partial z} = -C_{pul}\frac{\partial V}{\partial t}. \tag{2.18b}$$

Given these parameters, the *characteristic impedance*, Z_0, of the transmission line is given by

$$Z_0 = \sqrt{\frac{L_{pul}}{C_{pul}}}, \tag{2.19}$$

while the *propagation speed*, v_p, of the wave propagating along the line is given by

$$v_p = \left[\sqrt{L_{pul}C_{pul}}\right]^{-1}. \tag{2.20}$$

With these definitions in place, it is evident that wave propagation along a transmission line mirrors uniform plane-wave propagation in a dielectric medium.

To be able to simulate the transmission line structure, consider the one-dimensional representation with the voltage and current variables defined on a staggered grid, as shown in Figure 2.4.

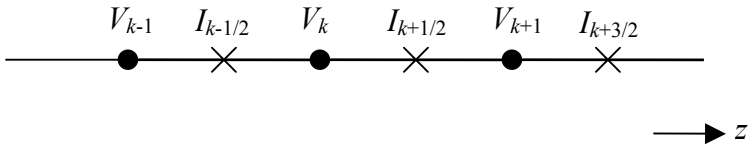

Figure 2.4: 1-D grid for transmission line showing staggered voltage and current variables.

Note that the voltage and current variables shown in Figure 2.4 are scalar quantities by construction. They are one-dimensional analogues to the electric and magnetic field existing in the dielectric of the transmission line structure. The current is related to the magnetic field via the relation

$$I_z = \Delta y \cdot H_y , \tag{2.21}$$

where we have assumed perfectly conducting metallization in the transmission line and Δy represents the width of the metallization in the y-direction. This current will then appear in an infinitely thin region along the edge of the metallization and will be distributed evenly along the width of the metallization.

2.3.3 Courant-Friedrichs-Lewy (CFL) stability criterion for the transmission line problem

In any explicit time-marching numerical integration scheme, the timestep used is limited by an unphysical, purely computational limit, beyond which the error will grow exponentially. This limit to the timestep is known as the Courant-Friedrichs-Lewy (CFL) stability criterion, and it was first observed by those authors in [11]. The exact limit depends on the time-marching algorithm, the physics of the underlying problem, and the spatial resolution [12]. For the case of wave propagation along a transmission line, it can be shown that the CFL criterion is given by the relation

$$\Delta t \leq \frac{\Delta z}{v_p} . \tag{2.22}$$

This effectively means that the timestep must be chosen so that the wave will not propagate beyond the length of one cell in the spatial discretization over the course of one timestep.

As a rule of thumb, the spatial discretization, characterized for the transmission line problem by Δz, is typically chosen to be at least 0.1 times the wavelength at the highest frequency of interest in the problem. Choosing the spatial discretization coarser than this limit will compromise the accuracy of the simulation.

This implies that FDTD simulation is a band-limited scheme – it is possible to accurately model frequencies only up to the limits of the discretization. The ideal transmission line, on the other hand, is an all-pass filter, with no limitations on the bandwidth of the input signal.

2.4 Methods for Combining Circuit Simulation and FDTD Simulation

Now that circuit simulation and FDTD simulation have each been reviewed independently, we briefly consider existing methods to combine the two in order to provide for hybrid EM/circuit cosimulation.

If we recall Maxwell's equations in Equations (2.14a-b), lumped circuit contributions into an FDTD simulation can be introduced via the impressed current source term $\mathbf{J}^i$ [4, 13-15]. This means that it is possible to directly incorporate the *i*-*v* relationship for circuit elements into the FDTD formulation. However this requires reformulating the *i*-*v* relationship for each element in terms of the FDTD equations and the Yee grid.

Alternatively, it is possible to directly link a circuit described by a SPICE-like netlist to a distributed structure simulated using FDTD [4, 16-19]. This is done by representing the distributed structure via a Norton equivalent circuit with a grid capacitance to account for stored charge in the FDTD lattice, as shown in Figure 2.5. While this does enable a hybrid simulation environment, the timesteps used in the distributed and lumped domains

are limited by the CFL stability criterion. The work presented in Chapter 4 is an improvement on these existing methodologies and enables the use of asynchronous time-integration methods. In particular, it enables the use of a timestep in the circuit domain that is not limited by the CFL stability criterion for FDTD.

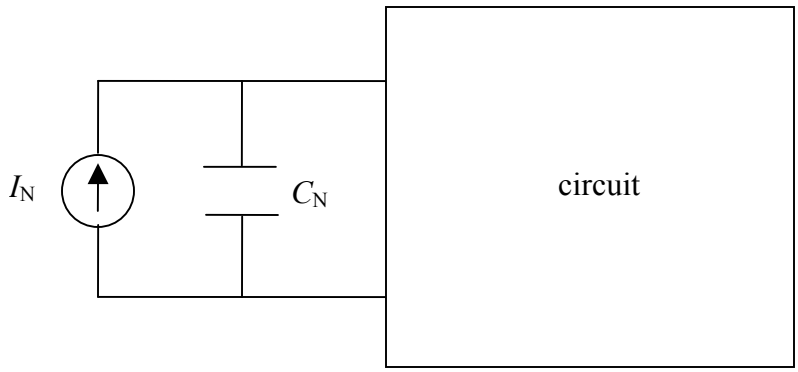

Figure 2.5: Norton equivalent for the interaction between FDTD grid and lumped circuit.

Meanwhile, asynchronous methods do exist for formulations other than FDTD. In particular, recent work has concentrated on time-domain integral-equation (TDIE) methods used in conjunction with circuit analysis to allow for hybrid EM/circuit simulation [20-23].

Alternatively, other attempts at the hybrid simulation problem assume a *circuit-centric* approach, whereby the distributed domain is converted into an equivalent circuit representation. The drawback to such an approach is that the full-wave electromagnetic model is lost in the resulting equivalent circuit. One consequence of this is that the resulting equivalent circuit is valid only over a fixed bandwidth. Nevertheless, this remains a popular approach to enabling hybrid EM/circuit cosimulation, and results of this type of methodology are used in this dissertation in conjunction with the methods introduced here.

CHAPTER 3

SPICE-COMPATIBLE STAMPS FOR THE NUMERICAL SIMULATION OF MAXWELL'S EQUATIONS IN THE TIME DOMAIN

3.1 Introduction

The previous chapter established that the SPICE simulation environment is an industry standard for the purpose of circuit analysis and design. Therefore, in the hybrid simulation of circuit and electromagnetic systems, it would be useful to describe the electromagnetic components in terms of a SPICE-equivalent circuit. It was also noted in the previous chapter that hybrid, time-domain electromagnetic/circuit simulators often assume a field-centric approach, whereby the electromagnetic field solver becomes the underlying simulation platform and the voltage/current state variables in the lumped circuit system are interfaced with the discrete electric and magnetic field variables defined on the finite-difference or finite-element grid through appropriately defined line integrals [4].

While this simulation approach is appropriate for those cases in which the lumped circuit components constitute an electrically small portion of the overall electromagnetic structure of interest, the reverse approach, namely, the incorporation of a semidiscrete electromagnetic model for a distributed portion of the structure under investigation within a circuit-based model of the structure, is also worth considering, especially in relation to the modeling of multiphysics phenomena involving multiple spatial scales of large disparity.

Among the numerous examples of models which can benefit from such modeling capability, some of the ones that prompted this work concern the development of phenomenological models for the exploration and quantification of various types of passive intermodulation (PIM) processes. As a specific example, shown in Figure 3.1 is a simplistic geometric representation of the electrical contact between two transmission lines. The nonlinearity of the constriction resistance at the contact [24, 25], and the possibility of tunneling through a very thin (< 100 Å) oxide layer formed between the contacts [26, 27], have been identified as potential sources of PIM. The quantification of the PIM effect requires a detailed enough model over the contact region that allows any relevant electromagnetic effects (e.g., heat generation due to ohmic loss and its impact on the temperature dependence of the constriction resistance) to be correctly accounted for, while also providing for the inclusion of nonlinear resistance and capacitance models for the tunneling effect. Clearly, an electromagnetic model becomes necessary, despite the electrically small size of the domain over which the aforementioned detailed modeling is applied. Furthermore, considering the fact that a significant number of linear/nonlinear circuit elements are included in the model, as well as the fact that thermal modeling may have to be carried out in a concurrent fashion, the utilization of a transient, circuit simulation environment is most suitable as the underlying simulation framework for our purposes.

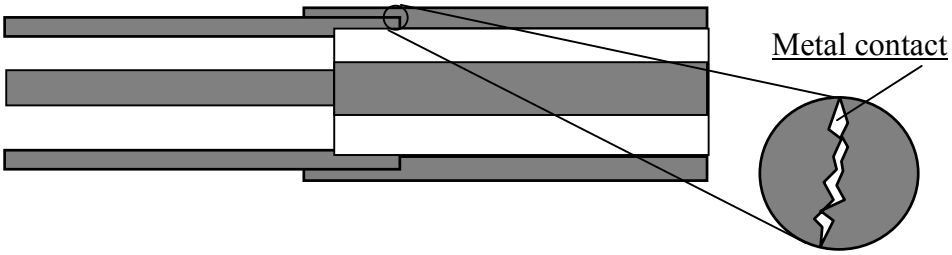

Figure 3.1: Generic geometry of a connection region between two transmission lines. Temperature-dependent constriction resistance and tunneling effects across very thin oxide layers at the metal contacts have been suggested as potential sources of PIM.

To provide for the direct incorporation of the semidiscrete (state-space) model resulting from the spatial discretization of Maxwell's equations, this chapter presents a methodology that leads to the representation of the semidiscrete systems in terms of stamps for the differential equations governing the temporal evolution of the discrete electric and magnetic field components. Of particular interest is the case where a uniform, rectangular Yee's lattice is utilized for the discretization of the curl operators in Maxwell's equations. For such a grid, the stamps assume fairly simple forms and can be expressed in terms of lumped circuit elements, coupled inductors, and dependent sources.

The organization of the chapter is as follows. First, the methodology used for the development of the equivalent circuit stamps is presented, adapted from [28]. This is followed by a validation of the method through the example of a rectangular cavity resonator with perfectly conducting walls. An analysis of the modes appearing in the resonator attests to the accuracy as well as some shortcomings of the methodology.

3.2 Methodology

The goal of the method proposed in this chapter is to enable the direct simulation of a distributed, electromagnetic structure using the SPICE circuit simulation environment. In

doing so, we do not want to introduce any numerical approximations other than those involved in the discretization of Maxwell's equations according to the rectangular Yee's lattice. In order to demonstrate how this is accomplished, begin by considering Maxwell's curl equations,

$$\nabla \times \mathbf{E} = -\mu \frac{\partial \mathbf{H}}{\partial t} \tag{3.1a}$$

$$\nabla \times \mathbf{H} = \sigma \mathbf{E} + \varepsilon \frac{\partial \mathbf{E}}{\partial t}. \tag{3.1b}$$

In the following paragraphs, these equations will be respectively identified as Faraday's and Ampère's laws.

Now, consider a semidiscrete approximation of these equations according to the rectangular Yee's lattice depicted in Figure 2.3. In other words, the spatial derivatives defined by the curl operators in Equations (3.1a-b) are computed along the discrete spatial grid introduced by the Yee's lattice, while the temporal derivatives of the field variables appearing on the right-hand side of Equations (3.1a-b) are left in a continuous form. Following this procedure, each component equation of Faraday's and Ampère's laws can be interpreted in terms of Kirchhoff's voltage and current laws. This is shown for one component of each of Faraday's and Ampère's laws as

$$\Delta x\left[E_x\left(i+\frac{1}{2}, j+1, k\right)-E_x\left(i+\frac{1}{2}, j, k\right)\right]+\Delta y\left[E_y\left(i, j+\frac{1}{2}, k\right)-E_y\left(i+1, j+\frac{1}{2}, k\right)\right]$$

$$=\Delta x \Delta y \mu \frac{\partial}{\partial t} H_z\left(i+\frac{1}{2}, j+\frac{1}{2}, k\right) \tag{3.2a}$$

$$\Delta x\left[H_x\left(i, j-\frac{1}{2}, k+\frac{1}{2}\right)-H_x\left(i, j+\frac{1}{2}, k+\frac{1}{2}\right)\right]+\Delta y\left[H_y\left(i+\frac{1}{2}, j, k+\frac{1}{2}\right)\right.$$

$$-H_y\left(i-\frac{1}{2},j,k+\frac{1}{2}\right)\Bigg] = \Delta x\Delta y\left(\sigma+\varepsilon\frac{\partial}{\partial t}\right)E_z\left(i,j,k+\frac{1}{2}\right). \quad (3.2b)$$

The other component equations can be written in a similar fashion by permuting the component indices and adjusting the spatial locations to satisfy the Yee's lattice.

Each such equation then has a natural interpretation in terms of lumped circuit stamps, shown for the cases of Equations (3.2a-b) in Figure 3.2. Again, the other component circuit stamps look very similar to the ones shown. In constructing these stamps, the electric field components are associated with node voltages, while the magnetic field components are associated with branch currents. It is important to note that this is merely a notational association between the field variables of Equations (3.2a-b) and the voltage nodes and current branches. In no way does this association imply any equivalence between them. Finally, upon constructing the stamps, the overall distributed structure is modeled by connecting the stamps together and linking them through dependent voltage and current sources.

3.3 Numerical Demonstration

We now consider an example in order to demonstrate the application of the equivalent circuit stamps described in the preceding section. The example uses the stamps to find transverse magnetic to z (TM^z) modes in a perfectly conducting, rectangular cavity resonator using the HSPICE simulation environment. This example is used to validate the accuracy of the proposed methodology.

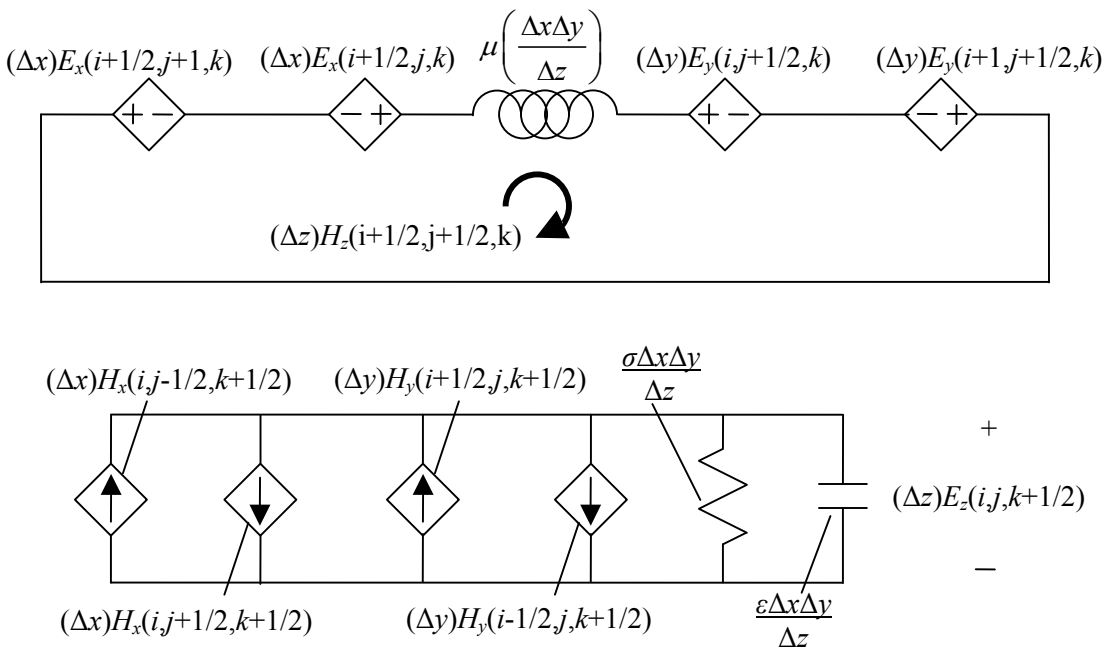

Figure 3.2: Equivalent circuit stamps for one component equation of each of Faraday's and Ampère's laws.

3.3.1 Rectangular cavity resonator

In order to validate the simulation of a distributed structure via use of the equivalent circuit stamps as described in the preceding section, consider the example of a rectangular cavity resonator with perfectly conducting walls. For the simulation problem, suppose the interior of this resonator consists of dielectric material with a permittivity of $\varepsilon = 2\varepsilon_0$ and permeability $\mu = \mu_0$. Also, suppose that the resonator has dimensions 0.1 m × 0.2 m × 0.2 m, discretized into 6 × 6 × 11 units in the x-, y-, and z-directions, respectively. Under this discretization, we expect to be able to capture modes with mode indices (1,1,0), (1,1,2), (1,3,0), and (1,3,2) with reasonable accuracy. Higher-order modes will not be sufficiently resolved under the given spatial sampling. The structure is excited with a z-directed current source located at the center of the domain with a bandwidth of 2.5 GHz.

This setup was simulated in the HSPICE environment, and the z-component of the electric field (identified by the appropriate node voltage modulated by the grid size in the z-direction) was measured at the location of the source. From this, it is possible to deduce the resonant frequencies of TM^z modes with odd x and y mode indices and even z mode index.

Figure 3.3 illustrates the results of a frequency sweep from DC to 2.5 GHz. For comparison, the analytic resonant frequencies of an ideal rectangular cavity resonator are shown as vertical dashed lines. We see that the first four modes are captured with an acceptable accuracy, whereas the fifth mode presents significantly greater dispersion. However, we did not expect to be able to capture that mode, as the discretization used was not fine enough to be able to accurately resolve such a high-order mode.

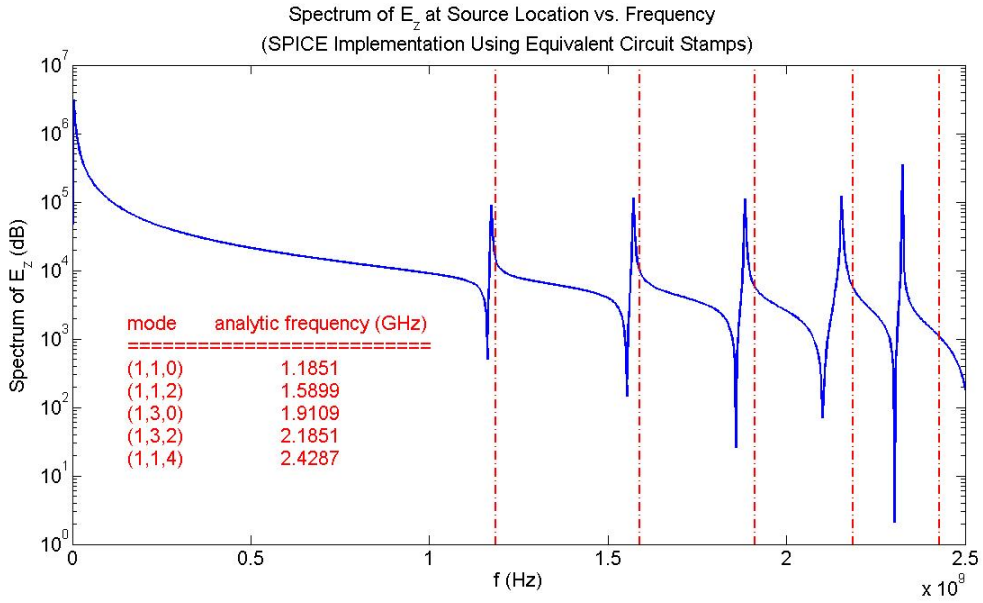

Figure 3.3: Spectrum of E_z at source location found using equivalent circuit stamps.

The result of the same simulation performed using the explicit time-marching standard FDTD scheme is shown in Figure 3.4. The results look somewhat better using this scheme than if the equivalent circuit stamps are used. That is, the standard FDTD scheme presents less numerical dispersion than the results using the equivalent circuit stamps.

Now, because the circuit stamps are an exact representation of Maxwell's equations with no added discretization errors beyond those introduced by the Yee's lattice and because the problem at hand is lossless (so there is no dispersion due to loss), it is concluded that the added dispersion in the proposed methodology is due to the numerical integration scheme used by HSPICE for the time integration of the equivalent circuit stamps. Presumably, HSPICE uses an unconditionally stable numerical integration scheme such as the backward Euler or trapezoidal rule. It is possible that HSPICE introduces some small losses into the equivalent circuit system so as to prevent resistance-free loops and nodes without a DC path to ground. However, if these losses are assumed small, they may not fully explain the discrepancies between the results using the equivalent circuit stamps and those using the explicit FDTD scheme. This then leads us to ponder why an implicit, unconditionally stable scheme should present greater dispersion than an explicit, conditionally stable scheme.

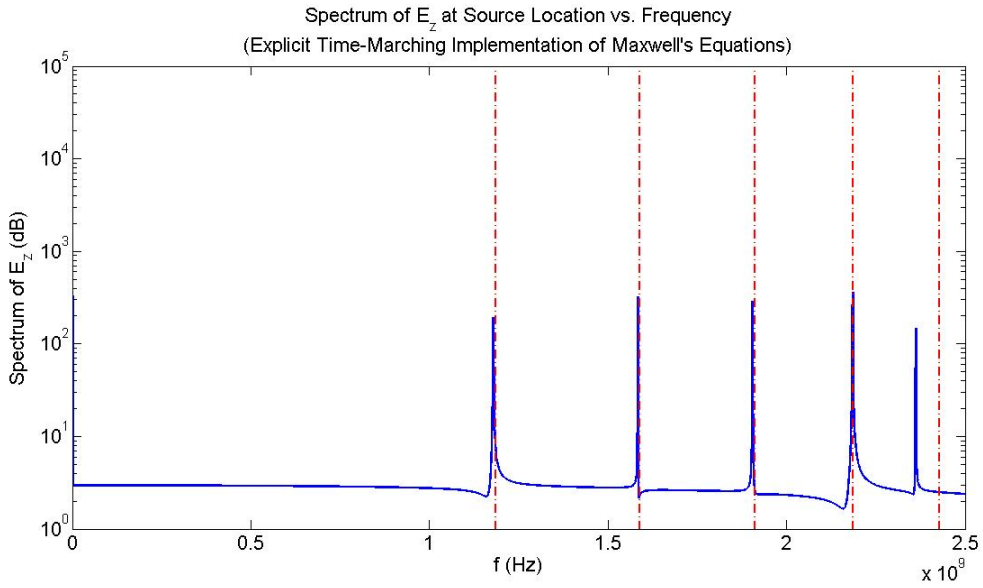

Figure 3.4: Spectrum of E_z at source location found using explicit time-marching scheme (standard FDTD).

3.3.2 Numerical dispersion relations

To get a better grasp on why one numerical integration scheme may result in less or more numerical dispersion than another, we undertake here a brief study of the dispersion relation of a general hyperbolic equation and the numerical dispersion relations of implicit and explicit schemes used in the numerical simulation of such an equation. In doing so, we hope to shed some light on the effect that a numerical integration scheme has on the accuracy of the solution to hyperbolic problems.

Consider a scalar function u satisfying the hyperbolic equation

$$u_{zz} - \frac{1}{c^2} u_{tt} = 0 . \tag{3.3}$$

This equation represents wave propagation in the z-direction in a lossless medium, where the constant c represents the propagation speed of the wave. The eigenfunctions of this equation (normalized for unit amplitude) are of the form

$$u = e^{j(\omega t - kz)}, \tag{3.4}$$

with the analytic dispersion relation

$$k = \frac{\omega}{c}. \tag{3.5}$$

Following the Fourier dispersion analysis method, utilize the discrete eigenfunction at spatial location $m\Delta z$ and temporal location $n\Delta t$, given by

$$u_m^n = e^{j(\omega n\Delta t - km\Delta z)}. \tag{3.6}$$

Substituting this function into Equation (3.3) following the appropriate discretization scheme and after some algebraic manipulation, the respective dispersion relations for the explicit FDTD and backward Euler schemes are derived:

$$\sin\left(\frac{k\Delta z}{2}\right) = \left(\frac{\Delta z}{c\Delta t}\right)\sin\left(\frac{\omega\Delta t}{2}\right) \tag{3.7a}$$

$$\sin\left(\frac{k\Delta z}{2}\right) = \left(\frac{\Delta z}{c\Delta t}\right)\tan\left(\frac{\omega\Delta t}{2}\right). \tag{3.7b}$$

The differences between the explicit FDTD and the backward Euler schemes are patent in the above relations. Specifically, it is clear that the timestep Δt in the explicit FDTD scheme is limited to $\Delta z/c$, but there is no such limit for the timestep used in backward Euler since the tangent function is unbounded. Also, note that if the timestep is chosen so as to satisfy the CFL stability criterion, then the explicit the explicit FDTD scheme has the same dispersion relation as the continuous wave equation. Therefore, the explicit FDTD method can provide dispersionless behavior, which is unattainable using other schemes.

CHAPTER 4

A DECOMPOSITION METHOD FOR THE SIMULATION OF HYBRID ELECTROMAGNETIC/CIRCUIT SYSTEMS WITH MULTIPLE TIME SCALES

4.1 Introduction

Recall that it was noted in Chapter 2 that the current approaches to the hybrid simulation of electromagnetic and circuit systems are not particularly suited to the cases when the electromagnetic structure constitutes only a small portion of the overall system under investigation. In particular, most current efforts toward circuit-centric solutions of the hybrid simulation problem do not directly discretize the Maxwell's system of equations but rather attempt to provide circuit-compatible, passive rational approximations to the electromagnetic subsystem [29]. The disadvantage to this approach is that the field-based model of the distributed components is lost, replaced by equivalent circuits that give meaningful values only at the ports.

The previous chapter addressed this deficiency by constructing equivalent circuit representations of Maxwell's equations discretized according to a Yee's lattice. These were then incorporated directly into a circuit-based description of the overall system.

This chapter takes on a slightly different approach by proposing a hybrid simulation methodology wherein each individual subsystem is simulated using a numerical integration scheme and a timestep that is most appropriate for the given physical characteristics of that subsystem. Following the traditional circuit-centric hybrid EM/circuit solution approach, it describes the different subsystems using a port-based

description. However, the values of the port characteristic for each subsystem are updated via numerical integration in the time domain. In this manner, hybrid systems involving multiple subsystems of varying spatial and time scales can be simulated in a global simulation.

The chapter begins with a description of the substitution theorem from classical network theory. A decomposition method from circuit theory known as waveform relaxation is then described, which leads to the methodology for the simulation scheme introduced in this chapter. This methodology involves two separate interpretations, by which the distributed portions are numerically integrated using either the standard FDTD scheme or an unconditionally stable Crank-Nicolson scheme. Examples are given to demonstrate the applications of these methods, followed by some concluding remarks.

4.2 Substitution Theorem from Network Theory

The basis of the hybrid simulation scheme developed in this chapter is the substitution theorem from classical network theory. A similar method was proposed for the purpose of harmonic balance simulation in [30], and this was extended to include circuit-field interactions as defined by the traditional network port-based description of the electromagnetic subsystem [31]. However, the disadvantage with the harmonic balance method is that because it is a frequency domain method, only mild nonlinearities are admitted. Performing simulations directly in the time domain allows the simulation of much stronger nonlinearities.

Consider an arbitrary network S that consists of two subnetworks S_1 and S_2 interconnected in a port-based manner, as shown in Figure 4.1. Furthermore, suppose

that the transfer voltage and current characteristic at the interface between the two subnetworks is known to be given by $v(t)$ and $i(t)$, respectively.

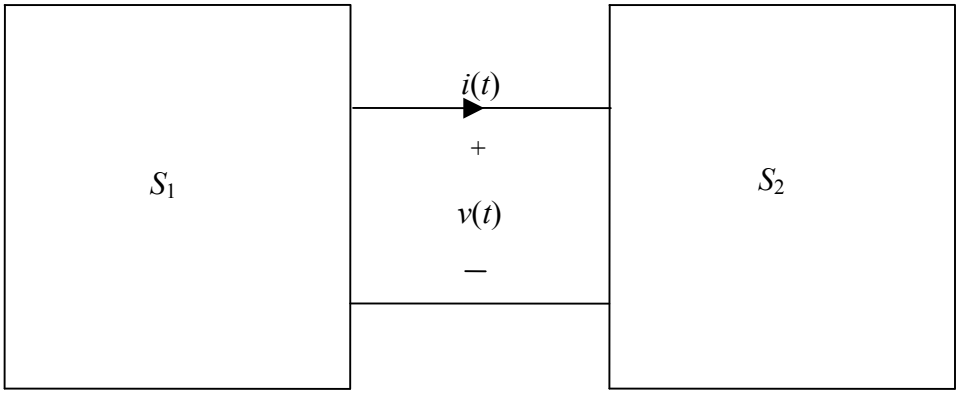

Figure 4.1: Arbitrary system S consisting of two subsystems S_1 and S_2 interconnected in a port-based manner.

Now, if neither of the two subnetworks contains any dependent sources that reference the value of a state variable in the other subnetwork, then the system S can be equivalently represented as shown in Figure 4.2, where the terminals of each subnetwork have been replaced by equivalent sources. Since the terminal voltage and current for each of S_1 and S_2 remain unchanged by this decomposition, it follows from the substitution theorem that all of the voltages and currents in each of the subnetworks S_1 and S_2 remain unchanged.

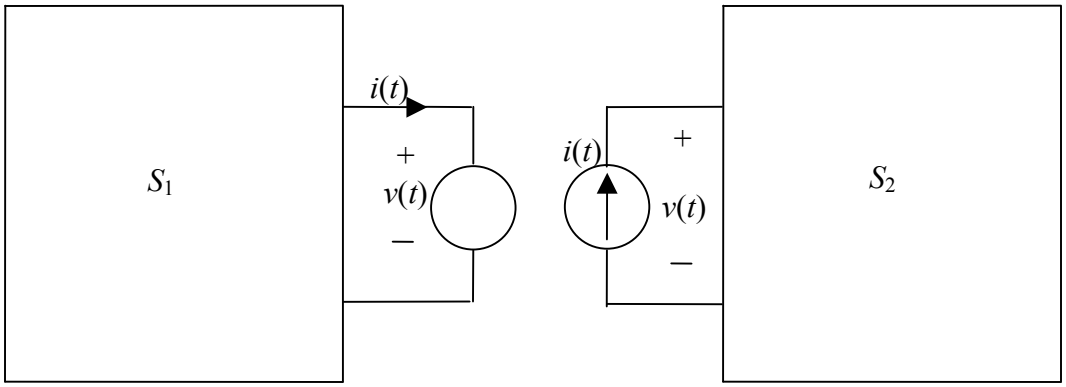

Figure 4.2: The substitution theorem from network theory allows the replacement of a port-based interconnection of subnetworks by voltage or current sources with the same time characteristic.

4.3 Waveform Relaxation

Waveform relaxation is a circuit simulation technique whereby the original circuit is manually partitioned into subcircuits. Each subcircuit is then individually solved over the time period of interest, and the overall solution is iteratively pieced together. Convergence is guaranteed following certain mild assumptions: namely, that there is a nonzero capacitance between each node and ground, and that the *i*–*v* or *q*–*v* characteristic for each element is Lipschitz continuous [2, 32, 33].

The advantage with the waveform relaxation method is that it allows the different subcircuits to be simulated at different timesteps. Thus, waveform relaxation is particularly suitable for performing timing analysis in circuits that exhibit an inherent latency in the signal propagation.

4.4 Methodology

The simulation scheme presented here is based on a modification to the equivalence described by the substitution theorem above. As will be seen below, the method is

similar to the waveform relaxation technique from circuit theory, except that there is only one iterate for each subsystem.

If a dependent voltage source v_1 is augmented to subsystem S_1, then denote the current flowing out of the terminals of S_1 (through v_1) by i_1. Now, if a dependent current source i_2 referencing the current i_1 is augmented to subsystem S_2, then define the voltage appearing at the terminals of S_2 by v_2. At each subsequent update in time for each subsystem, update the value of the appropriate source v_1 or i_2 based on the last known value of the equivalent voltage or current in the other subsystem. This is similar to a Gauss-Seidel relaxation process, whereby the last known value of any state variable is used to account for the interaction between different subsystems. This scheme is demonstrated pictorially in Figure 4.3.

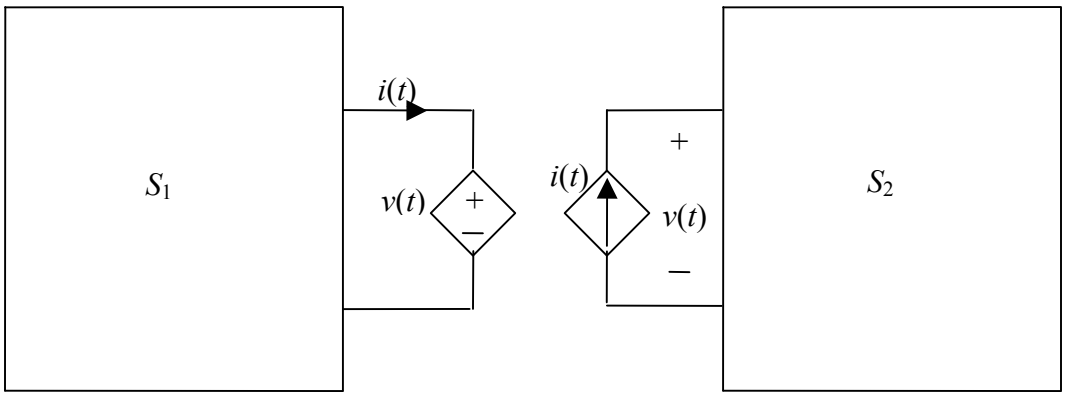

Figure 4.3: Decoupling of overall system via dependent sources. Each of S_1 and S_2 can now be updated using an integration scheme and timestep given the physical characteristics of each subsystem.

In this manner, the two subsystems are effectively decoupled and can then be integrated independently. This means that each subsystem can be numerically integrated using an integration scheme and timestep that is most appropriate given the physical

characteristics of that subsystem. Clearly, this method can be generalized to an arbitrary number of subsystems. Also, because sparse linear solvers scale superlinearly with the size of the system, this decomposition method is expected to be more efficient than performing the entire simulation using one global matrix. Most importantly, this method enables a direct, transient simulation of hybrid systems interconnected in a port-based manner without having to resort to any port-based approximations of any of the subsystems. This does not preclude the use of port-based data in any way, however.

4.5 Simulation Studies

Two numerical studies are now presented so as to validate the methodology described above. First, the simple example of a transmission line loaded with a lumped capacitor is used to illustrate the usage of the methodology. This is followed by the example of two parallel, short, coupled dipoles fed and loaded by transmission lines.

4.5.1 Transmission line with parallel *RC* load

Consider the simple example of a 10 cm long ideal, lossless transmission line with a characteristic impedance of 50 Ω and propagation velocity of 3×10^8 m/s, terminated by a lossy capacitive load consisting of the parallel combination of a matched 50 Ω resistor and a 5 pF capacitor. Then, the expected delay on the line would be 0.33 ns. Suppose that the source consists of a step voltage source with amplitude 5 V and a rise time of 0.15 ns, and allow the source impedance to be matched to the transmission line. This setup is shown in Figure 4.4.

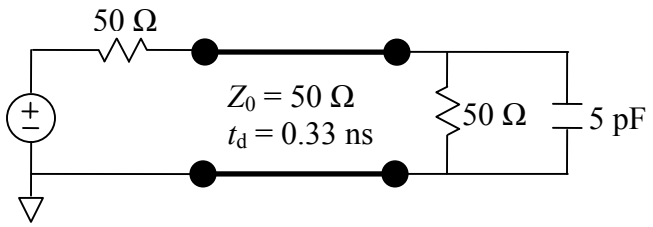

Figure 4.4: Transmission line with lossy capacitive load.

To facilitate the hybrid simulation, decompose this system into lumped and distributed portions. It is important to note that this decomposition is not based on the usual Norton equivalent representation of the distributed system with a grid capacitance [4]. Rather, the decomposition is based on the substitution theorem and replaces a subsystem having a given port characteristic with an equivalent dependent source. This decomposition is shown in Figure 4.5.

Because the load capacitor is large, the rate at which it charges is expected to be considerably slower than the rise rate of the source. Therefore, it is not necessary that the load circuitry be integrated using the same timestep as the wave propagation along the transmission line.

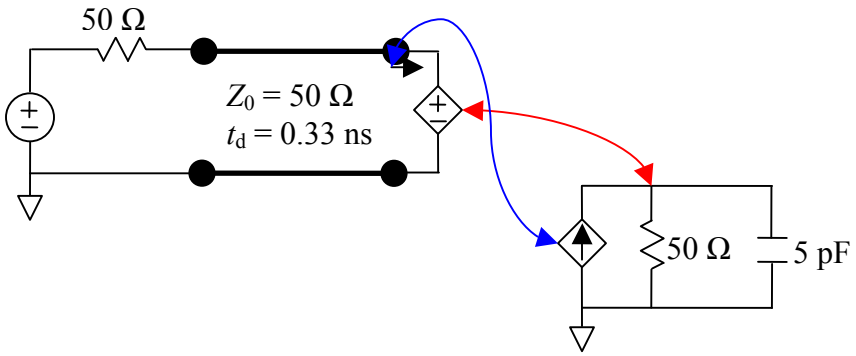

Figure 4.5: Decomposed transmission line system. The arrows show the associations of the dependent sources with their respective voltage nodes or current branches.

To illustrate the usage of the proposed scheme, the transmission line was discretized into a spatial grid consisting of $N_z = 100$ elements. This corresponds to approximately 20 points per wavelength for the given bandwidth of the input signal. Then the transmission line was simulated at a timestep equal to one-half the CFL limit via a standard explicit FDTD leapfrog scheme, while the load circuit was simulated at a timestep equal to 4 times the CFL limit, or 8 times the timestep used for the distributed portion. Clearly, the results, shown below in Figure 4.6, are of acceptable accuracy despite this difference in time scale used in the different subsystems.

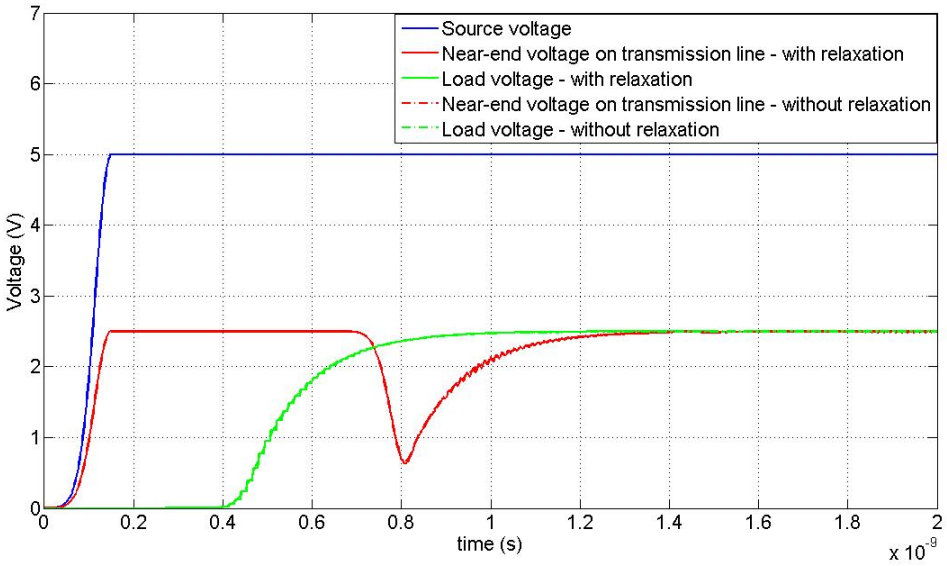

Figure 4.6: Propagation of voltage along a transmission line with lossy capacitive load.

4.5.2 Two short dipoles fed and loaded by matched transmission lines

Now consider the simulation setup shown in Figure 4.7, consisting of a circuit representation of two coupled short dipole antennas that is fed and loaded by matched transmission lines. Each antenna is 0.5 m in length, the antennas are 0.25 m apart, and

the antenna wire diameter is taken to be 50 mm. The admittance and impedance parameters were extracted for this pair of dipoles using the commercial software tool WIPL-D by treating the dipoles as a two-port system [34]. Using the impedance parameters, an equivalent circuit representation for the coupled antenna system was generated using the PRePFit algorithm [35-37], valid over the frequency range 0.1–1.0 GHz. The PRePFit algorithm applies passive rational fitting of the real part of a network transfer function to capture the resonances of the system and then casts the resulting rational approximation in the form of a SPICE equivalent circuit consisting of linear, passive elements. The size of the resulting SPICE circuit is 414 unknowns (in terms of voltage nodes and current branches).

As in the previous example, assume the transmission lines feeding and loading the dipoles are ideal and lossless, each with length 4 m, characteristic impedance 50 Ω, and propagation velocity of 3×10^8 m/s. Given these parameters, the expected delay in the line would be 13.33 ns. Also, assume the transmission lines are terminated with matched source and load impedances of 50 Ω.

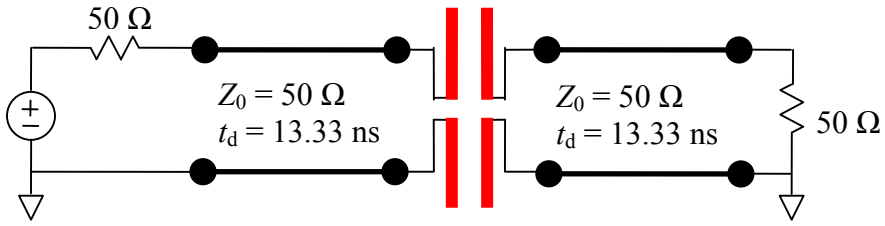

Figure 4.7: Two coupled dipole antennas fed and loaded by matched transmission lines.

Following the decomposition scheme, this system can be decomposed into separate lumped and distributed subsystems as shown in Figure 4.8.

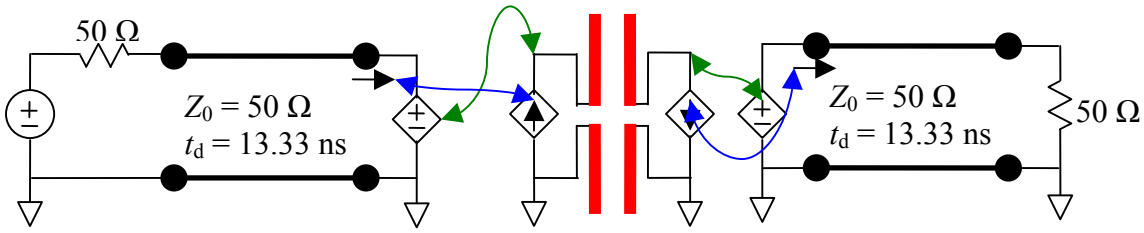

Figure 4.8: Decomposed system. The arrows show the associations of the dependent sources with their respective voltage nodes or current branches.

First, consider a 5 V step voltage source with a rise time of 8 ns powering the system. Using a rule-of-thumb approximation that the bandwidth BW of a step function with rise time T_r is given by $BW = 2/T_r$, the bandwidth of this signal will then be approximately 0.25 GHz. The problem is simulated by discretizing the transmission lines into $N_z = 200$ uniform segments, which corresponds to approximately 60 points per wavelength at the bandwidth of 0.25 GHz. The transmission lines are simulated using a standard explicit FDTD scheme using a uniform timestep of 33.33 ps, which is equivalent to a rate of half the CFL limit. A uniform timestep of twice the CFL limit, or 0.133 ns, was used to simulate the equivalent circuit representing the two dipoles. In other words, there is a factor of 4 between the two timesteps used in this simulation. The problem was simulated for a total time of 100 ns. The results of the simulation are shown in Figures 4.9 and 4.10 for voltages on the first transmission line and the second transmission line, respectively. Superimposed on each plot are the results if all subsystems are simulated using the same timestep of 33.33 ps, and it is evident that acceptable accuracy is seen when relaxing the timestep of the subcircuit representing the two dipoles. In each figure, the results labeled “with relaxation” refer to those results obtained when a different

timestep was used for simulating the lumped and distributed portions, whereas the results labeled “without relaxation” refer to the case when the same timestep was used.

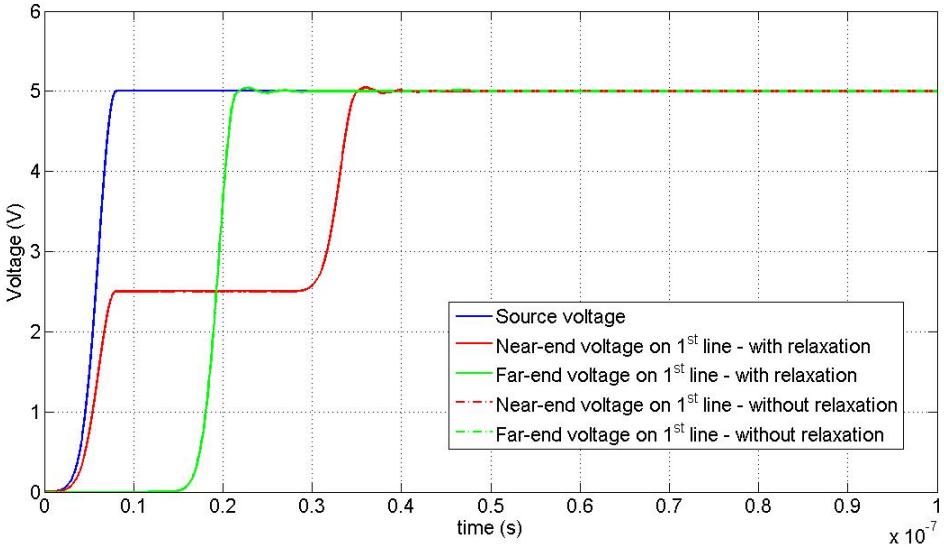

Figure 4.9: Voltages on the first transmission line, with and without relaxation.

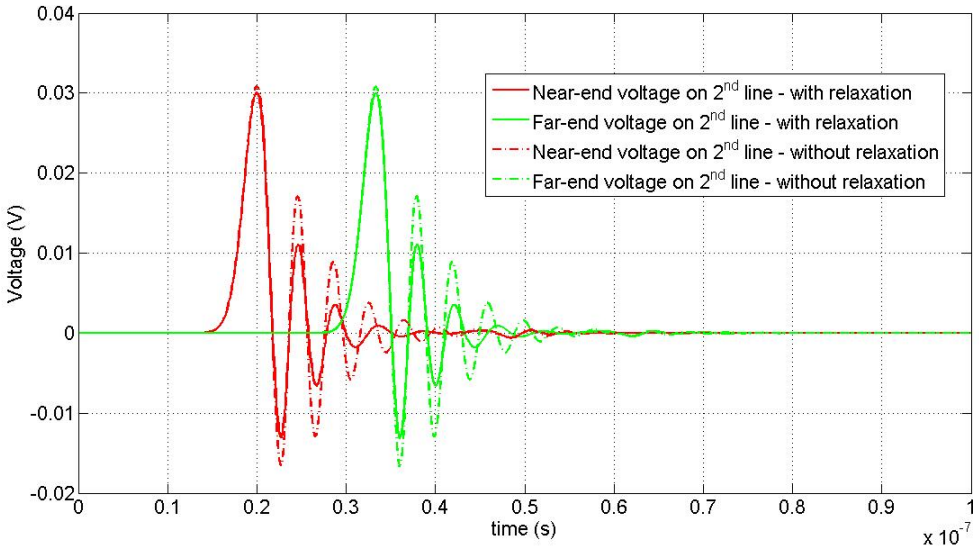

Figure 4.10: Voltages on the second transmission line, with and without relaxation.

In either case, there is only one iteration in the relaxation process during the transfer of information between the lumped and distributed domains at each time point in the simulation. This is in contrast to traditional waveform relaxation approaches, which solve for the entire time interval of simulation for each subsystem and then iterate on the continuity of boundary sources until convergence has been reached in all subsystems.

For this example, simulating the dipoles subcircuit at a rate of twice the CFL limit resulted in a savings of about 15% in the total runtime over the case when the dipoles subcircuit was simulated at half the CFL limit. The computer used was a Toshiba laptop with a Pentium 4 processor running Microsoft Windows XP. It is expected that the savings will be greater for a similar relaxation applied to a larger subcircuit.

Now, consider an input voltage source consisting of a 0.25 GHz sinusoid with amplitude 5 V that is modulated by a unit-strength Gaussian pulse centered at 32 ns with a width of about 10 ns. This waveform was used to simulate the same setup as before, and the results are shown below in Figures 4.11(a-b) and 4.12.

From Figure 4.11(b), it is evident that there is some reflection from the dipole pair at the frequency range of the input signal. Also, there is very little coupling onto the second dipole.

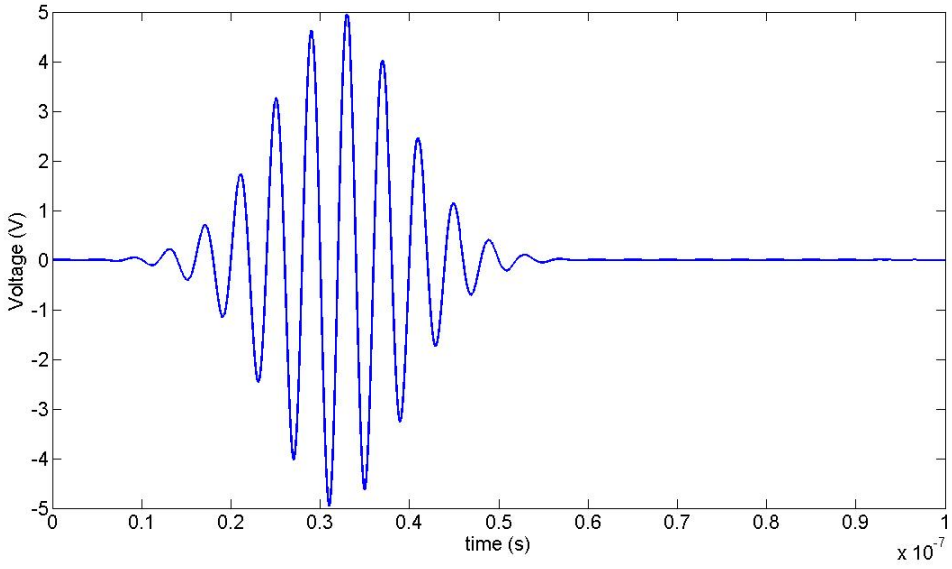

(a)

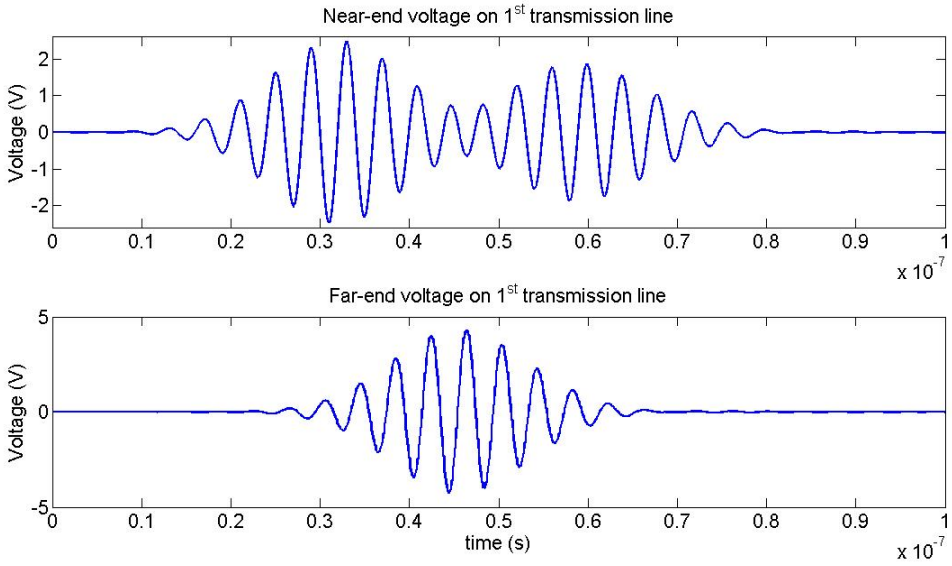

(b)

Figure 4.11: (a) Source voltage, (b) Near- and far-end voltages on the first transmission line, with relaxation.

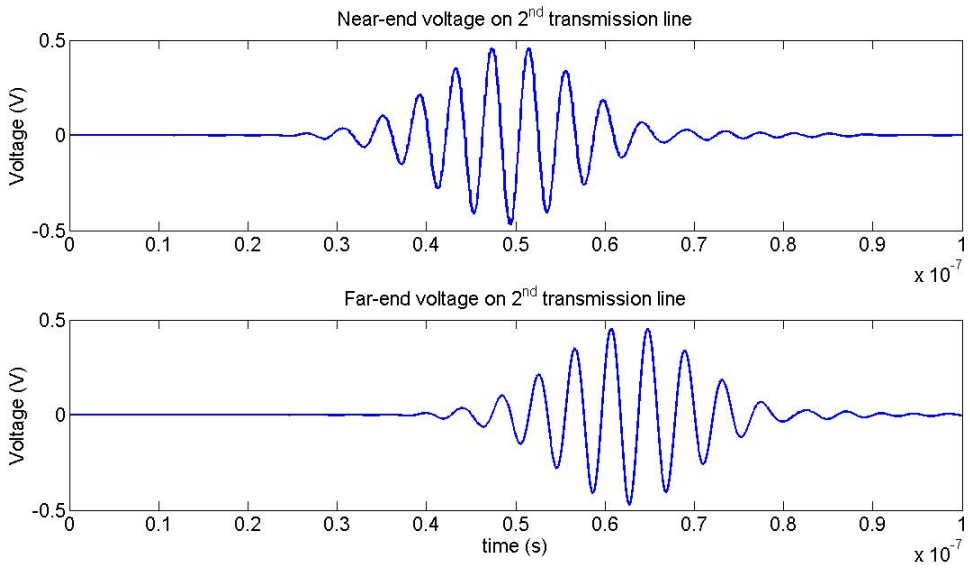

Figure 4.12: Voltages on the second transmission line, with relaxation.

4.5.3. Remarks

Based on numerical studies of this method, there are limitations on how far the timestep of the lumped portions can be pushed away from the CFL limit. Typically, instabilities will arise if the timestep is more than four times the CFL limit, although in some instances it is possible to push the timestep a little further. These instabilities are attributed (without proof) to the fact that the standard FDTD scheme is not always amenable to the zero-order-hold approximation that is done on the dependent sources at the boundary of the FDTD grid. This is because performing such an approximation interferes with the FDTD field updates.

In order to prevent instabilities, an unconditionally stable scheme may be utilized in the simulation of the transmission lines or other distributed portions. Two methods from circuit simulation immediately come to mind: the backward Euler and trapezoidal schemes. For the purpose of simulation of distributed structures, the trapezoidal method will be identified as the Crank-Nicolson method [38].

4.6 Unconditionally Stable Simulation of Transmission Lines

It was noted in the previous section that the standard, conditionally stable FDTD scheme may eventually result in some instabilities when combined with the hybrid simulation scheme introduced in this chapter if the timestep used for the simulation of the lumped portions exceeds the CFL limit significantly. Therefore, we now consider the simulation of wave-propagating structures such as transmission lines via unconditionally stable numerical integration schemes. As suggested in the previous paragraphs, two obvious choices for unconditionally stable integration are the backward Euler method and the Crank-Nicolson method. Certainly other methods exist, but these will be the ones considered here.

4.6.1 Choice of Crank-Nicolson versus backward Euler

It turns out that the backward Euler method is not particularly suitable for the simulation of wave propagation problems. To illustrate this point, consider the one-dimensional analogue of Ampère's law from the telegrapher's equations describing wave propagation along an ideal, lossless transmission line in Equation (2.18b), repeated here for convenience,

$$\frac{\partial I}{\partial z} = -C_{pul}\frac{\partial V}{\partial t}. \tag{4.1}$$

Now, as a crude approximation, the voltage variable V can be thought of as proportional to the current I by the characteristic impedance Z_0 of the transmission line given by Equation (2.19). This approximation is made disregarding the staggered spatial grid formed by the Yee's lattice and assuming unidirectional wave propagation, but it

will suffice to make the point here about the insufficiency of the backward Euler approximation.

To continue, it follows that the voltage variable approximately satisfies an equation of the form

$$\frac{\partial V}{\partial t} = -AV\,, \tag{4.2}$$

where the matrix A can be assumed to be diagonal provided an appropriate change of basis. In a physically realistic problem, the diagonal entries representing the eigenvalues of the system will be positive, meaning that A is a positive definite matrix. Now, if a backward Euler approximation is used on the time derivative operator in Equation (4.2), it follows that

$$V(n+1) - V(n) = -A\Delta t \cdot V(n+1)\,. \tag{4.3}$$

This can be written as an update equation as

$$V(n+1) = \frac{1}{1+a\Delta t} \cdot V(n)\,, \tag{4.4}$$

where a is a diagonal element of the characteristic matrix A. Equation (4.4) can again be rewritten as

$$V(n+1) = \left(\frac{1}{1+a\Delta t}\right)^{n+1} \cdot V(0)\,. \tag{4.5}$$

Now, notice that when a is large in magnitude, corresponding to a high-frequency response of the system, and Δt is not very small, the coefficient on the right-hand side of Equation (4.5) is small. In other words, the waveform may experience significant damping in time when the backward Euler method is used for the time discretization.

Alternatively, consider the results of the same process using the Crank-Nicolson scheme. Now the equation for the voltage variable reads

$$V(n+1)-V(n)=-\frac{A\Delta t}{2}\left[V(n+1)+V(n)\right]. \tag{4.6}$$

Again, writing an update equation gives

$$V(n+1)=\frac{1+a\Delta t/2}{1-a\Delta t/2}\cdot V(n), \tag{4.7}$$

which can be molded into

$$V(n+1)=\left(\frac{1+a\Delta t/2}{1-a\Delta t/2}\right)^{n+1}\cdot V(0). \tag{4.8}$$

Notice in this case that the coefficient on the right-hand side of Equation (4.8) is not damped out rapidly regardless of the value of the eigenvalue a or the timestep Δt — rather, it approaches -1. For this reason, the Crank-Nicolson method proves to be much more suitable for the simulation of transmission lines and other distributed structures, so it will be considered exclusively in the following sections.

4.6.2 Crank-Nicolson simulation of transmission lines

The Crank-Nicolson method effectively employs a trapezoidal integration of the distributed portions and therefore provides an unconditionally stable method to simulate hybrid structures. The unconditional stability arises from the implicitness of the scheme. Here, the method is developed for the simulation of the telegrapher's equations,

$$\frac{\partial V}{\partial z}=-L_{pul}\frac{\partial I}{\partial t} \tag{4.9a}$$

$$\frac{\partial I}{\partial z}=-C_{pul}\frac{\partial V}{\partial t}. \tag{4.9b}$$

Using the one-dimensional Yee's lattice to facilitate the discrete representation of the spatial derivatives and the Crank-Nicolson scheme for the time derivatives gives

$$\frac{V_p(m)-V_{p-1}(m)+V_p(m-1)-V_{p-1}(m-1)}{2\Delta z}=-\frac{L_{pul}}{\Delta t}\left[I_{p-1/2}(m)-I_{p-1/2}(m-1)\right] \tag{4.10a}$$

$$\frac{I_{p+1/2}(m)-I_{p-1/2}(m)+I_{p+1/2}(m-1)-I_{p-1/2}(m-1)}{2\Delta z}=-\frac{C_{pul}}{\Delta t}\left[V_p(m)-V_p(m-1)\right], \tag{4.10b}$$

where the subscripts refer to discrete locations along the spatial grid and the values in parentheses refer to discrete points along the temporal grid.

The feedback terms in the above equations provide for the unconditional stability of the scheme. In other words, the fact that the trapezoidal approximation to the time derivates couples the voltage and current variables together results in an unconditionally stable scheme.

Then, these equations can be assembled into a matrix equation with unknowns V and I as

$$[A]\cdot\begin{bmatrix}V(m)\\I(m)\end{bmatrix}=[b], \tag{4.11}$$

where

$$A = \begin{bmatrix} \frac{1}{2\Delta z} & & & \frac{L_{pul}}{\Delta t} & & & \\ -\frac{1}{2\Delta z} & \ddots & & & \ddots & & \\ & \ddots & \frac{1}{2\Delta z} & & & \ddots & \\ & & -\frac{1}{2\Delta z} & 0 & & & \frac{L_{pul}}{\Delta t} \\ \frac{C_{pul}}{\Delta t} & & & -\frac{1}{2\Delta z} & \frac{1}{2\Delta z} & & \\ & \ddots & & & \ddots & \ddots & \\ & & \frac{C_{pul}}{\Delta t} & & & -\frac{1}{2\Delta z} & \frac{1}{2\Delta z} \end{bmatrix}.$$

The vector *b* consists of the terms evaluated at time point $m-1$ in Equations (4.10a-b) as well as any sources that excite the ends of the transmission line. Therefore, the solution of the transmission line wave propagation can be thought of as the solution to the sparse matrix system in Equation (4.11) at each time point along the temporal grid.

In the following subsections, two examples are given in order to demonstrate the application of the Crank-Nicolson scheme to the simulation of transmission lines. The first of these examples serves as a numerical validation of the process and simply consists of a transmission line with a matched load. After that, the hybrid simulation of two dipoles fed and loaded by transmission lines is revisited.

4.6.3 Transmission line with matched load

To illustrate the advantages of the Crank-Nicolson integration method for simulating transmission lines, consider the simple example of a transmission line with matched load impedance. The characteristic impedance of the line is taken to be 50 Ω, and the source impedance is taken to be negligible. Also, assume that the wave propagates down the

line at a speed of 3×10^8 m/s. The source waveform is taken to be a Gaussian pulse centered in time at 0.6 ns and with a width of 0.2 ns. The discrete model of the transmission line is constructed so as to be able to support a bandwidth of 10 GHz, which is sufficient to support the Gaussian pulse that is exciting the line. Specifically, Δz is chosen to be 1/20 of the wavelength, assuming a maximum frequency of 10 GHz. The delay in the line is taken to be 1.2 ns, and as a result, the line is discretized spatially into 120 unit cells.

In Figure 4.13, the waveform appearing across the load impedance versus time is shown for four choices of timestep in the Crank-Nicolson simulation. The four timesteps used are multiples of 1, 2, 5, and 10 times the CFL stability limit governing a standard FDTD simulation of the same problem.

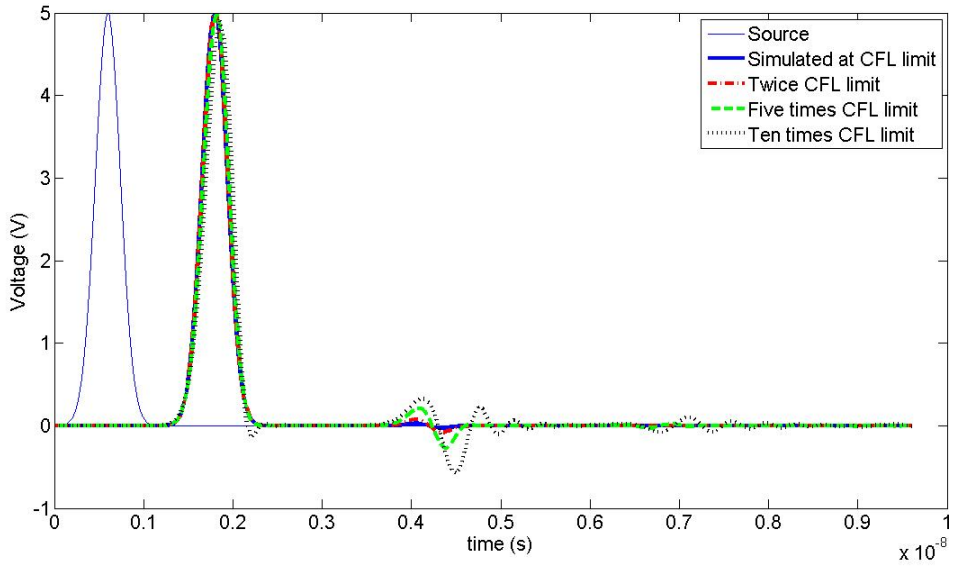

Figure 4.13: Gaussian waveform appearing at the load of a matched, lossless transmission line simulated using the Crank-Nicolson scheme at various timesteps.

Clearly, the Crank-Nicolson method is able to capture the waveform propagation along the transmission line quite accurately. However, as the timestep is increased well beyond the CFL limit, we see that there is slight dispersion in the resulting waveforms. In addition, some amount of ringing appears in the case that the timestep is chosen at ten times the CFL limit. This is attributed to the inability of that timestep to adequately capture the frequencies involved. Also, the reflections that are seen at the location of the load at a time point of around three times the one-way propagation delay are due to the zero impedance at the source. Nevertheless, it is evident that the Crank-Nicolson scheme lends a viable and efficient alternative to the standard FDTD method for the purpose of transmission line simulation.

4.6.4 Two short dipoles fed and loaded by matched transmission lines

In this section, the problem of two short dipoles fed and loaded by transmission lines that was studied using the hybrid simulation methodology in Section 4.5.2 is considered once again with the Crank-Nicolson method used for the simulation of the distributed components. The Gaussian-modulated sinusoid excitation used previously will be reused here.

This time, however, the transmission line is simulated using the Crank-Nicolson scheme at a timestep equal to the timestep used for the simulation of the equivalent circuit representing the two dipoles, which is equivalent to twice the CFL limit. Figures 4.14 and 4.15 show the results of this simulation. It is evident that a significant discrepancy exists between the results obtained using the Crank-Nicolson scheme and those obtained using the hybrid scheme of the previous section. There is a significant

level of signal amplitude variation, especially in the coupled waveforms. This can likely be improved by adjusting the timestep. The true cause of the discrepancy between the results shown here and those obtained previously is not entirely clear. Since the Crank-Nicolson scheme is a suitable method for the time integration of the distributed portion, the discrepancy most likely appears because of the handshake mechanism introduced in simulating the different components using dependent sources. Nevertheless, the advantage to this method lies in the computational savings. By using this method, a savings in simulation time of about 50% was realized over the hybrid simulation scheme performed earlier, even when relaxation was applied. However, further studies are needed to identify the true cause of the error appearing in the results and to propose methods to ameliorate the problem.

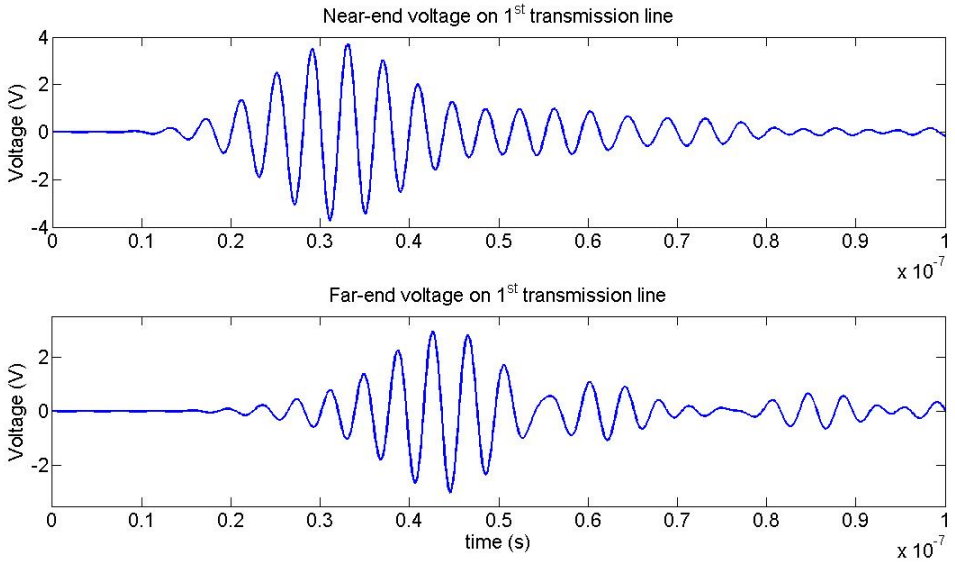

Figure 4.14: Voltage waveforms appearing on the first transmission line using the Crank-Nicolson scheme.

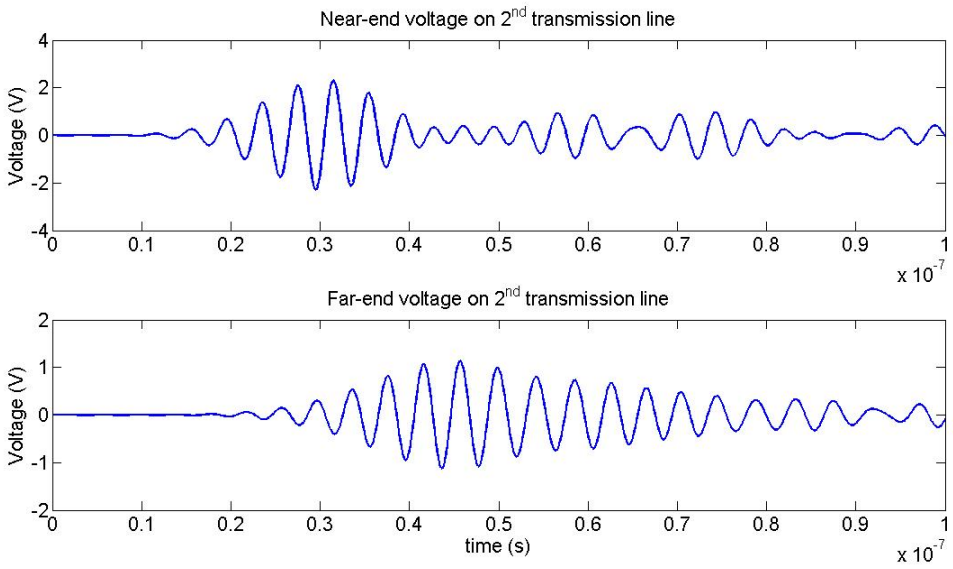

Figure 4.15: Voltages on the second transmission line using the Crank-Nicolson scheme.

4.7 Concluding Remarks

It is evident from the examples in the previous section that the method described in this chapter is computationally viable. The advantage that this method gives over existing approaches to hybrid FDTD/SPICE simulation is that the timestep used for the time integration of the circuit components is not limited by the CFL stability criterion that governs the timestep of the FDTD portions. However, when the standard FDTD method is used for the simulation of the distributed portions, the timestep chosen for the simulation of the lumped circuit components cannot be stretched indefinitely away from the CFL limit. Despite this limitation, some level of computational savings is witnessed by relaxing the timestep for the lumped subsystems.

Alternatively, an unconditionally stable implementation of the Crank-Nicolson scheme can be used to overcome the limitations on the timestep in the lumped portions. This provides additional savings in computational time. In this case, the timestep should

not be stretched too far beyond the CFL limit for the reason that numerical dispersion will appear in the propagating waveforms. The unconditional stability of the scheme used in both the lumped and distributed domains ensures that the outcome will be bounded regardless of the timestep used.

It must be noted, however, that the use of the Crank-Nicolson scheme along with the decomposition method proposed in this chapter does introduce significant spurious errors, the cause of which is not entirely clear. Further investigation is required in this direction to better understand the source of the errors.

Ultimately, these methods provide for novel ways to perform hybrid electromagnetic/circuit simulation and advance the current simulation methodologies in place in an attempt to allow for efficient global system simulation.

CHAPTER 5

THE ANALYSIS OF DISTRIBUTED CIRCUITS WITH WIDELY SEPARATED TIME SCALES USING MULTIVARIATE PDE METHODS

5.1 Introduction

This chapter deals with an efficient methodology for the transient analysis of circuits involving *multirate signals*, i.e., signals that contain frequency components that vary at two or more widely separated time scales. The method was most recently developed by Roychowdhury [39], although apparently the concept is not new and has been rediscovered more than once [40].

The problem with traditional circuit simulation methods in treating multirate signals arises from the separation in time scales. The timestep must be chosen small enough to capture the most rapidly varying signal components, which necessitates a very large number of time points to capture one period of the slowly varying components. The harmonic balance method is often used for the analysis of circuits demonstrating periodic behavior. However, harmonic balance is not suitable if strong nonlinearities are present.

Following the development in [39], the approach taken here is to efficiently represent such signals in the form of *multivariate functions* using two or more time variables. In this manner, time-domain methods can be used to solve for the unknowns directly in the multivariate formulation, thus allowing both strong nonlinearities and multirate behavior. In particular, we are concerned here with the application of this solution process to

distributed or transmission line circuits, characterized by wave propagation that is introduced by the presence of both inductive and capacitive elements.

5.2 Multivariate Representation of Multirate Signals

Consider a two-tone, quasi-periodic signal given by

$$b(t) = \sin(2\pi f_1 t)\sin(2\pi f_2 t), \tag{5.1}$$

where f_1 = 10 MHz and f_2 = 1 GHz. This means that 100 cycles of the rapidly varying sinusoid will be captured in the time needed to represent one cycle of the slowly varying sinusoid, as shown in Figure 5.1. In producing the plot in Figure 5.1, 15 points were used to represent each cycle of the rapidly varying sinusoid, meaning that 1500 points were needed to represent the entire plot. This represents a severe oversampling of the slowly varying signal, resulting in much redundancy of information and lack of efficiency in the solution process. In general, the total number of time points needed to represent one cycle of the slowly varying sinusoid while capturing the information in the rapidly varying sinusoid with acceptable accuracy is proportional to f_2/f_1.

In order to provide for a more compact representation of this type of signal, consider a multivariate representation of $b(t)$, whereby t is replaced by t_1 for the slowly varying components of $b(t)$ and t is replaced by t_2 for the rapidly varying components. The resulting bivariate representation is then a function of both t_1 and t_2,

$$\hat{b}(t_1, t_2) = \sin(2\pi f_1 t_1)\sin(2\pi f_2 t_2). \tag{5.2}$$

Note that $\hat{b}(t_1, t_2)$ is *biperiodic* in the sense that $\hat{b}(t_1 + T_1, t_2 + T_2) = \hat{b}(t_1, t_2)$, where T_1 = $1/f_1$ = 100 ns and $T_2 = 1/f_2$ = 1 ns. The multitime representation of $\hat{b}(t_1, t_2)$ is shown in

Figure 5.2, where 15 points are used to represent each period, resulting in just 225 samples.

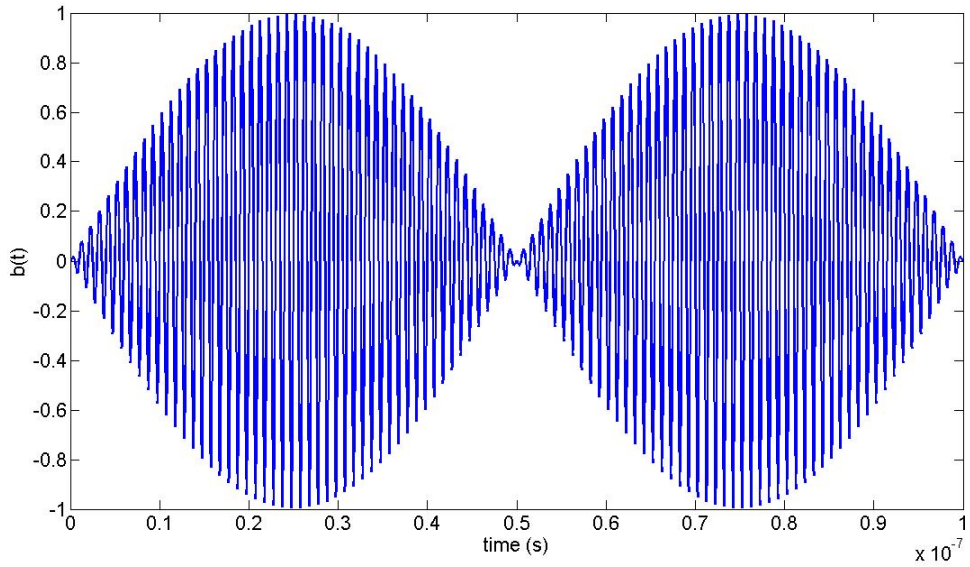

Figure 5.1: Multirate signal consisting of the product of two sinusoids with frequencies separated by a factor of 100.

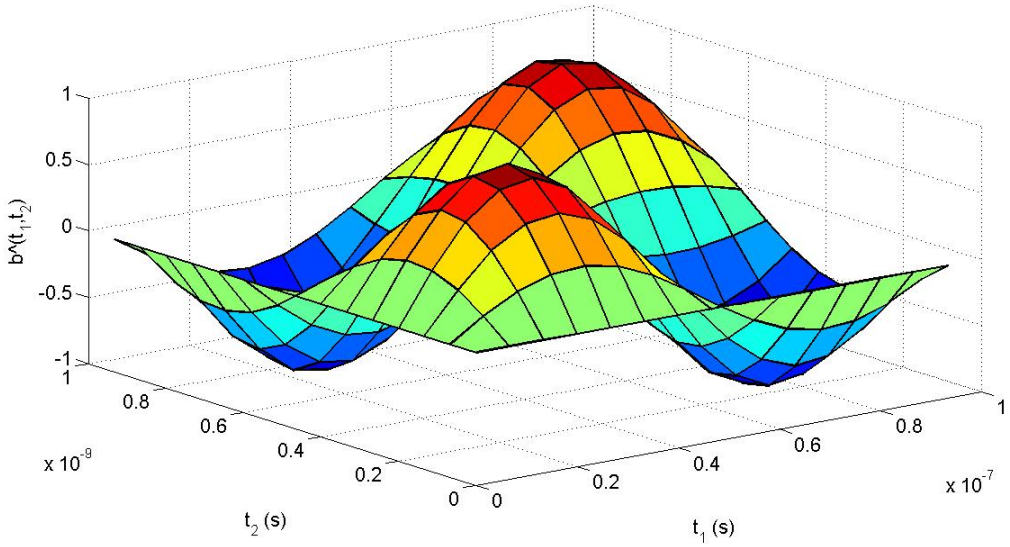

Figure 5.2: Bivariate representation of $b(t)$, represented using just 225 points.

Because of the biperiodic nature of $\hat{b}(t_1,t_2)$, it is easy to recover $b(t)$ given $\hat{b}(t_1,t_2)$ by simply setting $t_1 = t \bmod T_1$ and $t_2 = t \bmod T_2$,

$$b(t) = \hat{b}(t \bmod T_1, t \bmod T_2). \tag{5.3}$$

For example,

$$\begin{aligned} b(135.2 \text{ ns}) &= \hat{b}(135.2 \text{ ns}, 135.2 \text{ ns}) \\ &= \hat{b}(T_1 + 35.2 \text{ ns}, 135T_2 + 0.2 \text{ ns}) \\ &= \hat{b}(35.2 \text{ ns}, 0.2 \text{ ns}). \end{aligned}$$

As t increases from 0, the path given by $t_i = t \bmod T_i$ is traced by the sawtooth path shown in Figure 5.3.

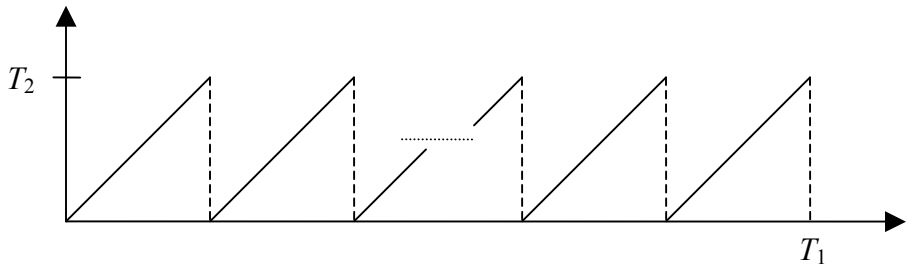

Figure 5.3: Sawtooth path traced by time in the t_1–t_2 plane.

5.3 The Multitime Partial Differential Equation (MPDE)

Consider a general circuit equation given by the following differential-algebraic equation (DAE),

$$\dot{q}(x) = f(x) + b(t), \tag{5.4}$$

where x represents the vector of unknowns. If the circuit exhibits multirate behavior, its variables can be represented efficiently using the multivariate representation described in the previous section with multiple time variables. Assuming M different time scales,

denote the multivariate representations of $x(t)$ and $b(t)$ by $\hat{x}(t_1,\ldots,t_M)$ and $\hat{b}(t_1,\ldots,t_M)$, respectively. Then the MPDE corresponding to Equation (5.4) for these multivariate forms is

$$\frac{\partial q(\hat{x})}{\partial t_1}+\cdots+\frac{\partial q(\hat{x})}{\partial t_M}=f(\hat{x})+\hat{b}(t_1,\ldots,t_M). \tag{5.5}$$

The sum of partial derivatives on the left-hand side of Equation (5.5) is due to the specific nature of the types of signals for which the MPDE formulation is valid. To be specific, the sum results from the application of the product rule in differentiation. The development in [39] provides several properties and theorems on the relation between the MPDE in Equation (5.5) and the original DAE in Equation (5.4). The key definitions and results are repeated here for the sake of completeness.

Theorem 5.1 (MPDE-DAE relation): If $\hat{x}(t_1,\ldots,t_M)$ and $\hat{b}(t_1,\ldots,t_M)$ satisfy the MPDE in (5.5), then $x(t)=\hat{x}(t+c_1,\ldots,t+c_M)$ and $b(t)=\hat{b}(t+c_1,\ldots,t+c_M)$ satisfy the DAE in (5.4) for any fixed $c_1,\ldots,c_M$.

Proof: Given $x(t)$ and $b(t)$ as stated in the theorem, it follows that

$$\begin{aligned}\dot{q}(x(t)) &= \frac{\partial q(\hat{x}(t+c_1,\ldots,t+c_M))}{\partial t}\\ &= \frac{\partial q(\hat{x})}{\partial t_1}+\frac{\partial q(\hat{x})}{\partial t_2}+\cdots+\frac{\partial q(\hat{x})}{\partial t_M}\\ &= f(\hat{x}(t+c_1,\ldots,t+c_M))+\hat{b}(t+c_1,\ldots,t+c_M)\\ &= f(x(t))+b(t).\end{aligned}$$

Q.E.D.

Boundary conditions need to be specified in order to solve the MPDE in Equation (5.5). Different sets of boundary conditions lead to either quasi-periodic or envelope-

modulated solutions. Some fundamental definitions and results for each of these cases are presented in the subsections below. Again, the treatment closely follows that given in [39].

5.3.1 Quasi-periodic signals

The concept of quasi-periodicity introduced earlier in this chapter via the prototypical signals in Equation (5.2) is now formalized by the following definition [39, 41].

Definition 5.1: A signal $y(t)$ is *M-tone quasi-periodic* if it can be expressed in the form

$$y(t) = \sum_{i_1,\ldots,i_M} Y(i_1,\ldots,i_M) \cdot \exp\left(j2\pi \left(\frac{i_1}{T_1} + \cdots + \frac{i_M}{T_M} \right) t \right)$$

where $Y(i_1,\ldots,i_M)$ are constants.

The concept of quasi-periodicity for univariate signals is closely related to periodicity for multivariate signals as shown by the definition and results below.

Definition 5.2: A multivariate signal $\hat{y}(t_1,\ldots,t_M)$ is *M-periodic* if

$$\hat{y}(t_1,\ldots,t_M) = \hat{y}(t_1 + k_1T_1,\ldots,t_M + k_MT_M)$$

for all real $t_1,\ldots,t_M$ and all integral values of $k_1,\ldots,k_M$. The constant real number T_i, i=1,…,M, is referred to as the *period of the* ith *tone* of $\hat{y}$, or simply the ith *period* of $\hat{y}$.

The following two lemmas show how to find a quasi-periodic, univariate signal $y(t)$ given an M-periodic signal $\hat{y}$ and vice versa.

Lemma 5.1: If $\hat{y}(t_1,\ldots,t_M)$ is M-periodic, then $y(t) = \hat{y}(t + c_1,\ldots,t + c_M)$ is M-tone quasi-periodic for any $c_1,\ldots,c_M$.

Proof: Expand $\hat{y}$ in a multidimensional Fourier series as

$$\hat{y}(t_1,\ldots,t_M) = \sum_{i_1,\ldots,i_M} Y(i_1,\ldots,i_M)\cdot\exp\left(j2\pi\left(\frac{i_1 t_1}{T_1}+\cdots+\frac{i_M t_M}{T_M}\right)\right).$$

The existence of such an expansion is guaranteed if we assume that $\hat{y}$ is sufficiently smooth with respect to each time variable $t_1,\ldots,t_M$. Then, it follows that

$$\begin{aligned} y(t) &= \hat{y}(t+c_1,\ldots,t+c_M) \\ &= \sum_{i_1,\ldots,i_M} Y(i_1,\ldots,i_M)\cdot\exp\left(j2\pi\left(\frac{i_1(t+c_1)}{T_1}+\cdots+\frac{i_M(t+c_M)}{T_M}\right)\right) \\ &= \sum_{i_1,\ldots,i_M}\left[Y(i_1,\ldots,i_M)\cdot\exp\left(j2\pi\left(\frac{i_1 c_1}{T_1}+\cdots+\frac{i_M c_M}{T_M}\right)\right)\right]\cdot\exp\left(j2\pi\left(\frac{i_1}{T_1}+\cdots+\frac{i_M}{T_M}\right)t\right). \end{aligned}$$

Therefore, it follows that $y(t)$ is M-tone quasi-periodic.

Q.E.D.

Lemma 5.2: Given an M-tone quasi-periodic function $y(t)$ and constants $c_1,\ldots,c_M$, there exists an M-periodic multivariate function $\hat{y}(t_1,\ldots,t_M)$ satisfying Lemma 5.1.

Proof: Since $y(t)$ is an M-tone quasi-periodic function, by definition it can be represented as

$$y(t) = \sum_{i_1,\ldots,i_M} Y(i_1,\ldots,i_M)\cdot\exp\left(j2\pi\left(\frac{i_1}{T_1}+\cdots+\frac{i_M}{T_M}\right)t\right).$$

Then, if we define the multivariate function $\hat{y}$ as

$$\begin{aligned} \hat{y}(t_1,\ldots,t_M) = \sum_{i_1,\ldots,i_M}&\left[Y(i_1,\ldots,i_M)\cdot\exp\left(-j2\pi\left(\frac{i_1 c_1}{T_1}+\cdots+\frac{i_M c_M}{T_M}\right)\right)\right] \\ &\cdot\exp\left(j2\pi\left(\frac{i_1 t_1}{T_1}+\cdots+\frac{i_M t_M}{T_M}\right)\right), \end{aligned}$$

it follows immediately that $\hat{y}(t+c_1,\ldots,t+c_M) = y(t)$.

Q.E.D.

The above results are now applied to the following theorem and corollary, which establish that an *M*-periodic solution to the MPDE in Equation (5.5) generates an *M*-tone quasi-periodic solution to the original DAE describing the circuit operation in Equation (5.4). These results follow immediately by applying the above two Lemmas to Theorem 5.1 and hence are given without proof.

Theorem 5.2 (MPDE sufficiency condition): If $\hat{b}$ is an *M*-periodic excitation and $\hat{x}$ is the *M*-periodic solution to the MPDE in (5.5), then $x(t) = \hat{x}(t + c_1, \ldots, t + c_M)$ is an *M*-tone quasi-periodic solution to the DAE in (5.4) with the *M*-tone quasi-periodic excitation given by $b(t) = \hat{b}(t + c_1, \ldots, t + c_M)$.

Corollary to Theorem 5.2: Given an *M*-periodic $\hat{b}$ and $b(t) = \hat{b}(t + c_1, \ldots, t + c_M)$, it is sufficient to find a solution $\hat{x}$ with *M*-periodic boundary conditions to the MPDE in Equation (5.5) in order to obtain an *M*-tone quasi-periodic solution $x(t) = \hat{x}(t + c_1, \ldots, t + c_M)$ to the DAE in Equation (5.4).

So far, we have established sufficiency conditions for the existence of an *M*-periodic solution of the MPDE to result in an *M*-tone quasi-periodic solution to the original DAE. Of equal importance is establishing the reverse necessity condition, which will maintain that any solution to the original DAE with an *M*-tone quasi-periodic excitation has a corresponding solution via the MPDE. This condition will ensure that no solution of the original DAE is lost by moving to the MPDE formulation, and it is established by the following theorem.

Theorem 5.3 (MPDE necessity condition): If an *M*-tone quasi-periodic solution $x(t)$ to the DAE in Equation (5.4) exists for a given *M*-tone quasi-periodic excitation $b(t)$, then

for any $c_1,\ldots,c_M$, there exist M-periodic functions $\hat{b}(t_1,\ldots,t_M)$ and $\hat{x}(t_1,\ldots,t_M)$ satisfying the MPDE in Equation (5.5) and such that $x(t)=\hat{x}(t+c_1,\ldots,t+c_M)$ and $b(t)=\hat{b}(t+c_1,\ldots,t+c_M)$.

Proof: Because $b(t)$ and $x(t)$ are quasi-periodic, they can be expressed as

$$b(t)=\sum_{i_1,\ldots,i_M} B(i_1,\ldots,i_M)\cdot\exp\left(j2\pi\left(\frac{i_1}{T_1}+\cdots+\frac{i_M}{T_M}\right)t\right)$$
$$x(t)=\sum_{i_1,\ldots,i_M} X(i_1,\ldots,i_M)\cdot\exp\left(j2\pi\left(\frac{i_1}{T_1}+\cdots+\frac{i_M}{T_M}\right)t\right).$$

The goal is to construct multivariate representations $\hat{b}$ and $\hat{x}$ of these signals that satisfy the MPDE. To do so, define

$$\hat{b}(t_1,\ldots,t_M)=\sum_{i_1,\ldots,i_M}\left[B(i_1,\ldots,i_M)\cdot\exp\left(-j2\pi\left(\frac{i_1c_1}{T_1}+\cdots+\frac{i_Mc_M}{T_M}\right)\right)\right]\cdot\exp\left(j2\pi\left(\frac{i_1t_1}{T_1}+\cdots+\frac{i_Mt_M}{T_M}\right)\right),$$

$$\hat{x}(t_1,\ldots,t_M)=\sum_{i_1,\ldots,i_M}\left[X(i_1,\ldots,i_M)\cdot\exp\left(-j2\pi\left(\frac{i_1c_1}{T_1}+\cdots+\frac{i_Mc_M}{T_M}\right)\right)\right]\cdot\exp\left(j2\pi\left(\frac{i_1t_1}{T_1}+\cdots+\frac{i_Mt_M}{T_M}\right)\right),$$

and note that $\hat{b}$ and $\hat{x}$ satisfy $b(t)=\hat{b}(t_1+c_1,\ldots,t_M+c_M)$ and $x(t)=\hat{x}(t_1+c_1,\ldots,t_M+c_M)$, respectively. Now, we can write the application of the functions $q(\bullet)$ and $f(\bullet)$ to $\hat{x}$ in the multivariate formulation as

$$q(\hat{x}(t_1,\ldots,t_M))=\sum_{i_1,\ldots,i_M}\hat{Q}(i_1,\ldots,i_M)\exp\left(j2\pi\left(\frac{i_1t_1}{T_1}+\cdots+\frac{i_Mt_M}{T_M}\right)\right)$$

and

$$f\left(\hat{x}\left(t_1,\ldots,t_M\right)\right)=\sum_{i_1,\ldots,i_M}\hat{F}\left(i_1,\ldots,i_M\right)\exp\left(j2\pi\left(\frac{i_1t_1}{T_1}+\cdots+\frac{i_Mt_M}{T_M}\right)\right).$$

Plugging in all of these terms into the DAE Equation (5.4) results in

$$\sum_{i_1,\ldots,i_M}\left[j2\pi\left(\frac{i_1}{T_1}+\cdots+\frac{i_M}{T_M}\right)\hat{Q}\left(i_1,\ldots,i_M\right)-\hat{F}\left(i_1,\ldots,i_M\right)-\hat{B}\left(i_1,\ldots,i_M\right)\right]\cdot\exp\left(j2\pi\left(\frac{i_1}{T_1}+\cdots+\frac{i_M}{T_M}\right)t\right)=0.$$

Now, in the case that $T_1,\ldots,T_M$ are pairwise incommensurate, meaning that no one of them is an integer multiple of another, each term in the above summation is equal to zero, so the MPDE is satisfied. In the more general case that the functions $\exp\left(j2\pi\left(\left(i_1/T_1\right)+\cdots+\left(i_M/T_M\right)\right)t\right)$ are not linearly independent of each other, it is necessary to generalize the idea. This is achieved by collecting together the linearly dependent terms in the summation. Denote by $\mathcal{M}$ the map from the indices to the frequencies,

$$\mathcal{M}:\left\{\left(i_1,\ldots,i_M\right)\right\}\mapsto\left\{2\pi\left(\frac{i_1}{T_1}+\cdots+\frac{i_M}{T_M}\right)\right\}.$$

Then, if $T_1,\ldots,T_M$ are mutually commensurate, it follows that the map $\mathcal{M}$ is not one-to-one. In other words, there are two sets of indices that map to the same frequency. Denote the range of $\mathcal{M}$ by Ω, consisting of a countable set of distinct frequencies ω_k. For any $\omega_k\in\Omega$, let I_k be the set of all indices $(i_1,\ldots,i_M)$ that map to ω_k; i.e., $I_k=\mathcal{M}^{-1}(\omega_k)$. If $T_1,\ldots,T_M$ are pairwise incommensurate, then I_k is a set of cardinality one; otherwise, it is a countably infinite set. Note that according to this definition of I_k, if $\omega_k\neq\omega_l$, then

$I_k \bigcap I_l = \varnothing$. Using this fact, group together the indices that reside in each I_k and write the DAE as

$$\sum_k \left[\sum_{(i_1,\ldots,i_M)\in I_k} \left[j2\pi \left(\frac{i_1}{T_1} + \cdots + \frac{i_M}{T_M} \right) \hat{Q}(i_1,\ldots,i_M) - \hat{F}(i_1,\ldots,i_M) - \hat{B}(i_1,\ldots,i_M) \right] e^{j\omega_k t} \right] = 0 .$$

In the above relation, the functions $e^{j\omega_k t}$ are linearly independent by construction, so the coefficients must be zero,

$$\sum_{(i_1,\ldots,i_M)\in I_k} \left[j2\pi \left(\frac{i_1}{T_1} + \cdots + \frac{i_M}{T_M} \right) \hat{Q}(i_1,\ldots,i_M) - \hat{F}(i_1,\ldots,i_M) - \hat{B}(i_1,\ldots,i_M) \right] = 0 .$$

The above equation is equivalent to requiring the DAE to be satisfied. But the requirement to satisfy the MPDE is somewhat stronger, as each term in the above summation must individually be equal to zero. This requirement cannot be satisfied by the current definition of $\hat{b}$. It is necessary, therefore, to take advantage of the fact that in the commensurate case, many different multivariate forms of $\hat{b}$ and $\hat{x}$ can correspond to the same univariate function. In this light, redefine $\hat{b}$ using a different set of quasi-periodic coefficients as

$$\tilde{B}(i_1,\ldots,i_M) = \left[j2\pi \left(\frac{i_1}{T_1} + \cdots + \frac{i_M}{T_M} \right) \hat{Q}(i_1,\ldots,i_M) - \hat{F}(i_1,\ldots,i_M) \right] \cdot \exp\left(j2\pi \left(\frac{i_1 c_1}{T_1} + \cdots + \frac{i_M c_M}{T_M} \right) \right) .$$

Note that this definition of $\tilde{B}(i_1,\ldots,i_M)$ does satisfy the DAE requirement as before, so it follows that $\tilde{b}(t)$ and $x(t)$ satisfy the original DAE. Now, define $\hat{\tilde{b}}(t_1,\ldots,t_M)$ as

$$\hat{\tilde{b}}(t_1,\ldots,t_M)=\sum_{i_1,\ldots,i_M}\left[\tilde{B}(i_1,\ldots,i_M)\exp\left(-j2\pi\left(\frac{i_1c_1}{T_1}+\cdots+\frac{i_Mc_M}{T_M}\right)\right)\right.$$
$$\left.\cdot\exp\left(j2\pi\left(\frac{i_1t_1}{T_1}+\cdots+\frac{i_Mt_M}{T_M}\right)\right)\right].$$

From this definition, it follows that $\tilde{b}(t)=\hat{\tilde{b}}(t+c_1,\ldots,t+c_M)$ is equal to

$$\tilde{b}(t)=\sum_k\left[\sum_{(i_1,\ldots,i_M)\in I_k}\left[j2\pi\left(\frac{i_1}{T_1}+\cdots+\frac{i_M}{T_M}\right)\hat{Q}(i_1,\ldots,i_M)-\hat{F}(i_1,\ldots,i_M)\right]e^{j\omega_k t}\right],$$

which can be simplified to

$$\begin{aligned}\tilde{b}(t)&=\sum_k\left[\sum_{(i_1,\ldots,i_M)\in I_k}\hat{B}(i_1,\ldots,i_M)e^{j\omega_k t}\right]\\&=\sum_{i_1,\ldots,i_M}\hat{B}(i_1,\ldots,i_M)\cdot\exp\left(j2\pi\left(\frac{i_1}{T_1}+\cdots+\frac{i_M}{T_M}\right)t\right).\\&=b(t)\end{aligned}$$

Hence, $\hat{\tilde{b}}(t+c_1,\ldots,t+c_M)=b(t)$. Finally, it needs to be shown that $\hat{\tilde{b}}(t_1,\ldots,t_M)$ and $\hat{x}(t_1,\ldots,t_M)$ satisfy the MPDE. By substituting the multivariate expressions for these variables into the MPDE, it is found that

$$\sum_{i_1,\ldots,i_M}\left[j2\pi\left(\frac{i_1}{T_1}+\cdots+\frac{i_M}{T_M}\right)\hat{Q}(i_1,\ldots,i_M)-\hat{F}(i_1,\ldots,i_M)-\hat{\tilde{B}}(i_1,\ldots,i_M)\right]$$
$$\cdot\exp\left(j2\pi\left(\frac{i_1t_1}{T_1}+\cdots+\frac{i_Mt_M}{T_M}\right)\right)=0$$

The coefficients of the expression above are seen to be zero by substituting in the definition of $\hat{\tilde{B}}(i_1,\ldots,i_M)$, and hence, the MPDE is satisfied.

Q.E.D.

Therefore, we have established a bijective correspondence between solutions to the original DAE in Equation (5.4) and the MPDE in Equation (5.5) under the assumption of the existence of at least one such solution. This ensures that solutions found to the system under the MPDE formulation can indeed be found to correspond to a solution to the original DAE and vice versa.

However, in general, neither the existence nor the uniqueness of a solution to the MPDE can be guaranteed. For that matter, the existence or uniqueness of a quasi-periodic signal to the DAE cannot be guaranteed either. This can be verified by considering the equation $\dot{x} = 1 + \cos(t)$, which has no quasi-periodic solutions, or the equation $\dot{x} = 0$, which has an infinite number of (constant) quasi-periodic solutions.

5.3.2 Envelope-modulated signals

An *envelope-modulated* signal with $M - 1$ periodic components can be represented in multivariate form as

$$\hat{x}(t_1,\ldots,t_M) = \sum_{i_2,\ldots,i_M} X_{i_2,\ldots,i_M}(t_1)\cdot\exp\left(j2\pi\left(\frac{i_2 t_2}{T_2}+\cdots+\frac{i_M t_M}{T_M}\right)\right). \tag{5.6}$$

In the above representation, $\hat{x}$ is periodic with respect to each of its arguments except for t_1, which in practice is usually chosen as the variable with the slowest rate. The univariate representation is then in the form of a Fourier series with time-varying envelopes in the variable t_1. With this interpretation, an envelope-modulated signal can be thought of as a generalization of the quasi-periodic representation of the previous subsection in the sense that the space of quasi-periodic signals is a subset of the space of envelope-modulated signals.

The envelope solutions to the MPDE in the form of Equation (5.6) require both an initial condition in the variable t_1 and periodic boundary conditions in the other variables $t_2,\ldots,t_M$. In other words, envelope-modulated solutions to the MPDE require that $\hat{x}(0,t_2,\ldots,t_M)$ is specified as well as T_i-periodic boundary conditions for each argument t_i for $i=2,\ldots,M$. The following theorem ensures the uniqueness of a solution satisfying these conditions.

Theorem 5.4 (Uniqueness of envelope solution): If the DAE in Equation (5.4) has a unique solution given any initial condition, then the solution $\hat{x}(t_1,\ldots,t_M)$ of the MPDE is also unique with the initial and periodic boundary conditions $\hat{x}(0,t_2,\ldots,t_M)=h(t_2,\ldots,t_M)$ and $\hat{x}(t_1,t_2,\ldots,t_M)=\hat{x}(t_1,t_2+T_2,\ldots,t_M+T_M)$, where h is any given initial condition.

Proof: It follows from Theorem 5.1 that solutions to the MPDE along the "diagonal lines" given by $\hat{x}(t,t+c_2,\ldots,t+c_M)$ are exactly the solutions to the DAE with initial condition $h(c_2,\ldots,c_M)$. Now, since the DAE has a unique solution with $h(c_2,\ldots,c_M)$ specified, it follows that the MPDE has a unique solution along the diagonal lines passing through $(0,c_2,\ldots,c_M)$. Since the solution to the MPDE is periodic along the directions $t_2,\ldots,t_M$, it follows that the MPDE has a solution along the diagonal lines. Therefore, the solution to the MPDE is unique.

Q.E.D.

In solving for envelope-modulated solutions to the MPDE, the initial condition is chosen to be a quasi-periodic solution to the circuit at $t_1=0$ so that the envelope function changes gradually as a function of t_1.

At this point, the discrete (numerical) time-domain solution methodology is developed for the MPDE in Equation (5.5) for each of the two cases of quasi-periodic signals as well as envelope-modulated signals.

5.4 Time Domain Solution to the MPDE

Time domain solutions are particularly useful when strong nonlinearities are present in the signal path. This section develops two time-domain solution methodologies for the MPDE: the multivariate FDTD (MFDTD) method for quasi-periodic solutions, and the time domain envelope method (TD-ENV) for envelope-modulated solutions. Other possible solution methodologies exist, including hierarchical shooting (HS) in the time domain as well as the multivariate mixed frequency-time method (MMFT) [39], but these will not be considered in this thesis.

5.4.1 Multivariate FDTD method (MFDTD)

First consider the solution of the MPDE for the case of quasi-periodic excitations. In order to simplify the development, consider the two-rate case, i.e., $M = 2$. Then the MPDE of Equation (5.5) becomes

$$\frac{\partial q\left(\hat{x}\right)}{\partial t_1} + \frac{\partial q\left(\hat{x}\right)}{\partial t_2} = f\left(\hat{x}\right) + \hat{b}\left(t_1, t_2\right), \tag{5.7}$$

subject to the periodic boundary conditions

$$\hat{x}\left(t_1 + T_1, t_2 + T_2\right) = \hat{x}\left(t_1, t_2\right). \tag{5.8}$$

The problem unknowns are collocated over a uniform grid $\left\{\overline{t}_{m,n}\right\}$ of size $N = N_1 \times N_2$ on the rectangle $[0,T_1]\times[0,T_2]$, where $\overline{t}_{m,n} = \left(t_{1,m}, t_{2,n}\right)$ with $t_{1,m} = (m-1)h_1$, $t_{2,n} = (n-1)h_2$, $h_1 = T_1/N_1$, $h_2 = T_2/N_2$, $1 \le m \le N_1$, $1 \le n \le N_2$.

Assume, without loss of generality, that $T_1 \gg T_2$ and that $N_1 \approx N_2$. Then, define a *multivariate trapezoidal approximation* for the MPDE in Equation (5.7),

$$\begin{aligned}
&\frac{q\left(\hat{x}\left(\overline{t}_{m,n}\right)\right) - q\left(\hat{x}\left(\overline{t}_{m-1,n}\right)\right)}{2h_1} + \frac{q\left(\hat{x}\left(\overline{t}_{m,n-1}\right)\right) - q\left(\hat{x}\left(\overline{t}_{m-1,n-1}\right)\right)}{2h_1} + \\
&\frac{q\left(\hat{x}\left(\overline{t}_{m,n}\right)\right) - q\left(\hat{x}\left(\overline{t}_{m,n-1}\right)\right)}{2h_2} + \frac{q\left(\hat{x}\left(\overline{t}_{m-1,n}\right)\right) - q\left(\hat{x}\left(\overline{t}_{m-1,n-1}\right)\right)}{2h_2} = \\
&\frac{1}{4}\Big[f\left(\hat{x}\left(\overline{t}_{m,n}\right)\right) + \hat{b}\left(\overline{t}_{m,n}\right) + f\left(\hat{x}\left(\overline{t}_{m-1,n}\right)\right) + \hat{b}\left(\overline{t}_{m-1,n}\right) + \\
&\qquad f\left(\hat{x}\left(\overline{t}_{m,n-1}\right)\right) + \hat{b}\left(\overline{t}_{m,n-1}\right) + f\left(\hat{x}\left(\overline{t}_{m-1,n-1}\right)\right) + \hat{b}\left(\overline{t}_{m-1,n-1}\right)\Big].
\end{aligned} \tag{5.9}$$

In the above equation, the average between values at time points $\overline{t}_{m,n}$, $\overline{t}_{m-1,n}$, $\overline{t}_{m,n-1}$ and $\overline{t}_{m-1,n-1}$ is necessary to accurately solve for the unknowns in the transmission line circuits that are of interest in this dissertation. Without the time averaging (or a similar approximation), a significant amount of numerical dispersion appears in simulating a transmission line circuit. This is because of the hyperbolic nature of the wave propagation along a transmission line. In general, *LC*-type circuits cannot accurately resolve narrowband signals using a backward Euler approximation. Thus, a trapezoidal-type rule must be used for hyperbolic systems. This fact was established in Chapter 4 for the case of univariate solution methodologies to transmission line circuits.

Applying the biperiodic boundary conditions in Equation (5.8) results in *N* equations in *N* unknowns, multiplied by the size of the circuit. Because of the sparse structure of the coefficient matrix, sparse matrix solvers can be utilized for the solution. The solution

process directly discretizes and solves for one period in each of the time scales. While this has the advantage of not involving time-stepping because of the direct enforcement of the periodic boundary conditions, it does result in a somewhat larger system. Therefore, the efficiency of the solution process is largely dependent on the size of the original circuit and the total time over which the transient simulation is needed.

5.4.2 Time domain envelope following method (TD-ENV)

Now consider the solution of the MPDE for the case of envelope-modulated excitation signals. As mentioned earlier, this class of signals is a generalization of the quasi-periodic signals, in the sense that quasi-periodic signals can be analyzed using the techniques from this solution methodology. However, a wider class of signals is also admitted; namely, signals for which one "direction" does not necessarily exhibit periodic behavior.

Again, for reasons of simplicity, consider the case when $M = 2$. Then the circuit unknowns can be described in bivariate form as $\hat{x}(t_1, t_2)$, and the MPDE of Equation (5.5) can be written as

$$\frac{\partial q(\hat{x})}{\partial t_1} + \frac{\partial q(\hat{x})}{\partial t_2} = f(\hat{x}) + \hat{b}(t_1, t_2), \tag{5.10}$$

subject to the boundary conditions

$$\begin{aligned} \hat{x}(t_1, t_2 + T_2) &= \hat{x}(t_1, t_2) \\ \hat{x}(0, t_2) &= h(t_2) \end{aligned}. \tag{5.11}$$

In Equation (5.11) above, h is some initial condition defined along t_1=0.

Again, the problem unknowns are collocated over a uniform grid $\{\overline{t}_{m,n}\}$ of size $N = N_1 \times N_2$ on the rectangle $[0,T_1]\times[0,T_2]$, where $\overline{t}_{m,n} = (t_{1,m}, t_{2,n})$ with $t_{1,m} = (m-1)h_1$, $t_{2,n} = (n-1)h_2$, $h_1 = T_1/N_1$, $h_2 = T_2/N_2$, $1 \le m \le N_1$, $1 \le n \le N_2$. However, in this case, T_1 need not represent a physical period, since the multivariate representations do not necessarily display periodic behavior in the t_1-direction for the case of envelope-modulated signals. Rather, T_1 now represents the total simulation time over which the solution is to be found.

Proceeding as in the previous subsection, define the *multivariate trapezoidal approximation* for the MPDE in Equation (5.10) as

$$\begin{aligned}
&\frac{q\left(\hat{x}\left(\overline{t}_{m,n}\right)\right)-q\left(\hat{x}\left(\overline{t}_{m-1,n}\right)\right)}{2h_1}+\frac{q\left(\hat{x}\left(\overline{t}_{m,n-1}\right)\right)-q\left(\hat{x}\left(\overline{t}_{m-1,n-1}\right)\right)}{2h_1}+\\
&\frac{q\left(\hat{x}\left(\overline{t}_{m,n}\right)\right)-q\left(\hat{x}\left(\overline{t}_{m,n-1}\right)\right)}{2h_2}+\frac{q\left(\hat{x}\left(\overline{t}_{m-1,n}\right)\right)-q\left(\hat{x}\left(\overline{t}_{m-1,n-1}\right)\right)}{2h_2}=\\
&\frac{1}{4}\Big[f\left(\hat{x}\left(\overline{t}_{m,n}\right)\right)+\hat{b}\left(\overline{t}_{m,n}\right)+f\left(\hat{x}\left(\overline{t}_{m-1,n}\right)\right)+\hat{b}\left(\overline{t}_{m-1,n}\right)+\\
&\qquad f\left(\hat{x}\left(\overline{t}_{m,n-1}\right)\right)+\hat{b}\left(\overline{t}_{m,n-1}\right)+f\left(\hat{x}\left(\overline{t}_{m-1,n-1}\right)\right)+\hat{b}\left(\overline{t}_{m-1,n-1}\right)\Big].
\end{aligned} \tag{5.12}$$

Because the time-stepping is performed in the first time variable t_1, the discretized MPDE of Equation (5.12) can be written as an update equation in t_1,

$$\begin{aligned}
&\frac{q\left(\hat{x}\left(\overline{t}_{m,n}\right)\right)+q\left(\hat{x}\left(\overline{t}_{m,n-1}\right)\right)}{2h_1}+\frac{q\left(\hat{x}\left(\overline{t}_{m,n}\right)\right)-q\left(\hat{x}\left(\overline{t}_{m,n-1}\right)\right)}{2h_2}\\
&-\frac{1}{4}\Big[f\left(\hat{x}\left(\overline{t}_{m,n}\right)\right)+\hat{b}\left(\overline{t}_{m,n}\right)+f\left(\hat{x}\left(\overline{t}_{m,n-1}\right)\right)+\hat{b}\left(\overline{t}_{m,n-1}\right)\Big]=\\
&\frac{1}{4}\Big[f\left(\hat{x}\left(\overline{t}_{m-1,n}\right)\right)+\hat{b}\left(\overline{t}_{m-1,n}\right)+f\left(\hat{x}\left(\overline{t}_{m-1,n-1}\right)\right)+\hat{b}\left(\overline{t}_{m-1,n-1}\right)\Big]\\
&+\frac{q\left(\hat{x}\left(\overline{t}_{m-1,n}\right)\right)+q\left(\hat{x}\left(\overline{t}_{m-1,n-1}\right)\right)}{2h_1}-\frac{q\left(\hat{x}\left(\overline{t}_{m-1,n}\right)\right)-q\left(\hat{x}\left(\overline{t}_{m-1,n-1}\right)\right)}{2h_2}.
\end{aligned} \tag{5.13}$$

Now, at each time point along the t_1-axis, a system of size N_2 times the size of the circuit must be solved. In the more general case of M time variables, the system size that must be solved at each step along t_1 is $N_2 \times \cdots \times N_M$ times the size of the circuit. Because the size of the system in this case is reduced by a factor of N_1 relative to the size of the system in the MFDTD solution methodology, the TD-ENV provides considerable savings in computational time for larger circuits. Additionally, because the time scale t_1 most often represents the most slowly varying scale (longest period), it is possible to discretize just that time scale but still cover a long range in time, which provides considerable computational savings over the traditional, univariate solution methodology.

5.5 Application to Transmission Line Circuits

The MFDTD and TD-ENV solution methodologies developed in the previous sections will now be used to study wave propagation along transmission lines. First, an ideal, lossless transmission line will be considered, followed by an investigation of wave propagation along a transmission line with periodically varying dielectric properties.

5.5.1 Ideal lossless transmission line

Consider the circuit shown in Figure 5.4, representing an ideal, lossless transmission line. The inductance and capacitance values are given by $L = L_{pul} \cdot \Delta z$ and $C = C_{pul} \cdot \Delta z$, respectively, where L_{pul} and C_{pul} are respectively the per-unit-length inductance and capacitance of the line. The values of L_{pul} and C_{pul} are chosen so that the speed of wave propagation along the line is $v_p = 3 \times 10^8$ m/s and the characteristic impedance of the line is $Z_0 = 50\ \Omega$:

$$L_{pul} = \frac{Z_0}{v_p},\ C_{pul} = \frac{1}{Z_0 v_p}. \tag{5.14}$$

The spatial discretization Δz is chosen as 1/20 of the minimum wavelength, which is the wavelength at the sum of the two frequencies of the multirate signal that serves as the excitation for the line. For the purpose of this example, the source voltage assumes the values for the signal given in section 5.2, which was a quasi-periodic signal with frequency components of f_1 = 10 MHz and f_2 = 1 GHz. The total length of the simulated line is taken to be 9 wavelengths at the minimum wavelength, resulting in a one-way propagation delay of about 8.91 ns. Each of the two periods is collocated over 15 points; i.e., $N_1 = N_2 = 15$. This means that the size of the resulting matrix system for the MFDTD method will be 225 times the number of state variables in the original circuit.

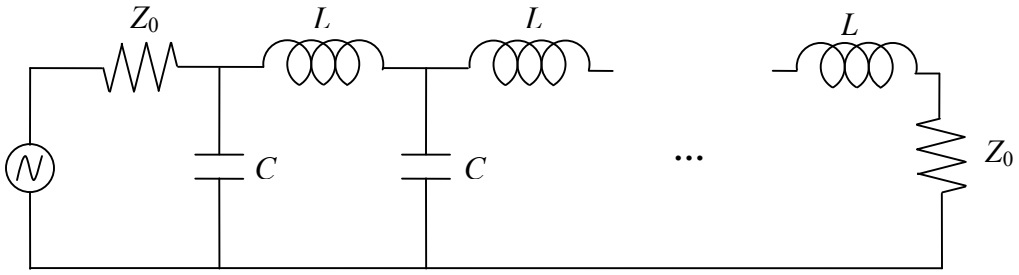

Figure 5.4: Circuit representing an ideal, lossless transmission line with matched source and load impedances.

The waveforms appearing at the midpoint and load of the transmission line as a result of simulating this circuit using the MFDTD methodology presented in the previous section are shown in Figures 5.5 and 5.6. It should be noted that the waveforms shown in those figures have been linearly extrapolated onto a finer time scale than the one used in the solution process. This is done to make easier the comparison with the results of a

traditional, univariate circuit simulation method. It is apparent that the results are reasonably accurate, with only a small amount of dispersion present. Because the method assumes a periodic variation of all signals, periodic boundary conditions are enforced. This means that the propagation delay is captured as a phase shift in the output waveforms with respect to the source waveform.

Obviously then, the maximum delay that can be captured by this scheme is T_1, and delays greater than this will be represented modulo T_1. However, for long transmission lines, the size of the problem becomes prohibitive because of lack of available memory, making the MFDTD method not particularly useful in these instances.

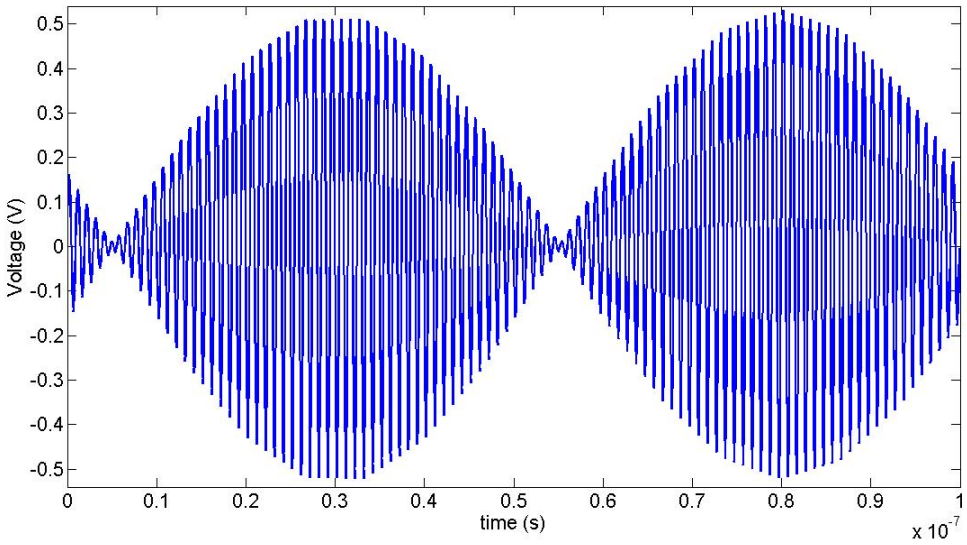

Figure 5.5: Voltage waveform appearing at the midpoint of the transmission line simulated using the MFDTD method.

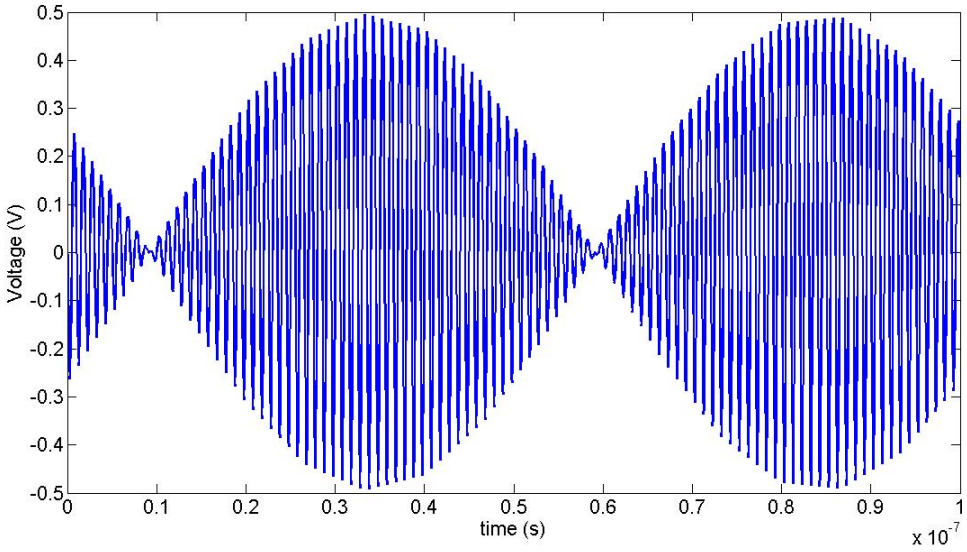

Figure 5.6: Voltage waveform appearing at the load of the transmission line simulated using the MFDTD method.

The results of the same simulation performed using the TD-ENV method are shown in Figures 5.7 and 5.8. Because the lowest-frequency component is treated as an envelope to the higher-frequency components in this case, these waveforms do not appear as phase-shifted versions of the input. This is because periodic boundary conditions are not applied to the low-frequency component. For the purpose of this simulation, the low-frequency envelope was simulated at a rate of 20 points per period, which is slightly denser than the discretization of the low-frequency component in the MFDTD simulation.

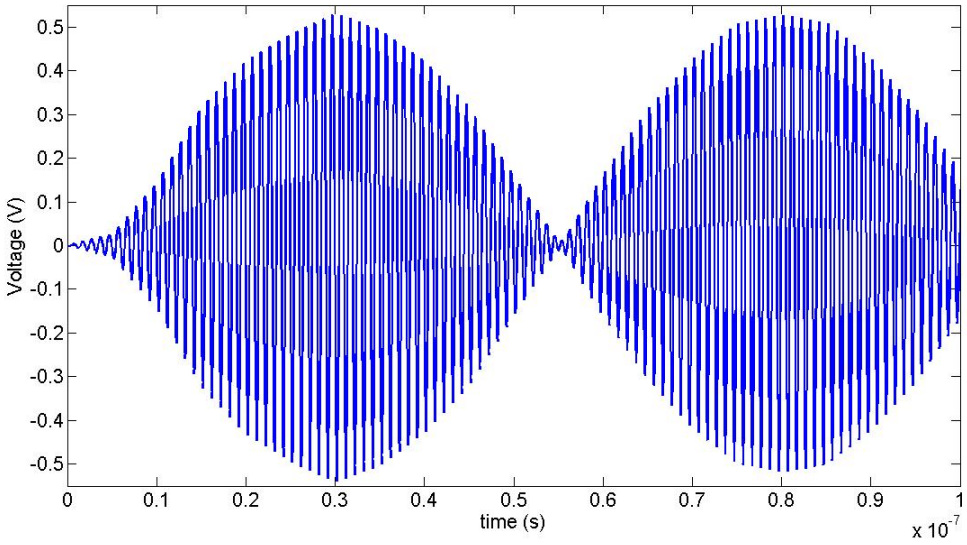

Figure 5.7: Voltage waveform appearing at the midpoint of the transmission line simulated using the TD-ENV method.

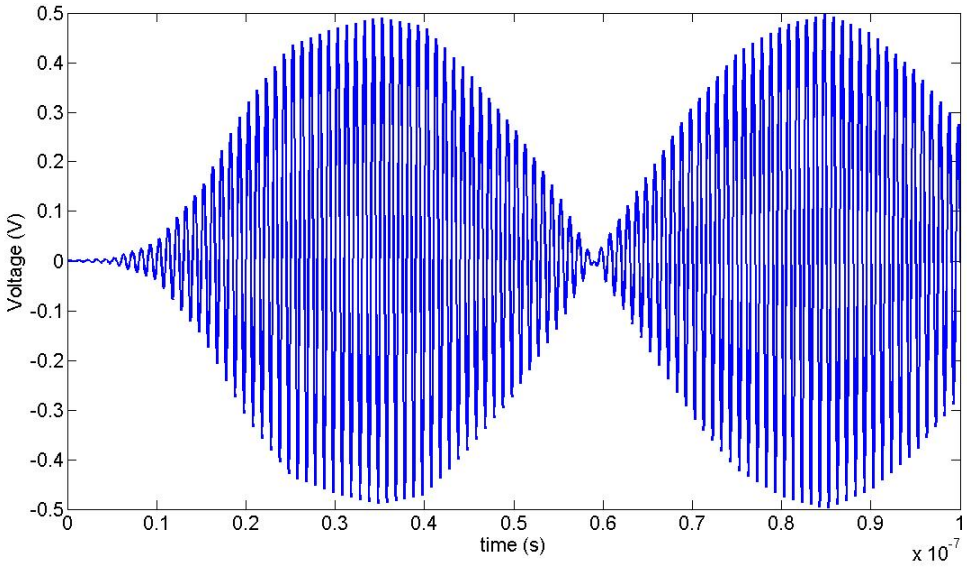

Figure 5.8: Voltage waveform appearing at the load of the transmission line simulated using the TD-ENV method.

For comparison, the results of the same simulation performed using a single-time trapezoidal circuit simulation scheme (akin to a Crank-Nicolson simulation of the transmission line) are shown next. Figure 5.9 gives the result at the midpoint of the

transmission line, and Figure 5.10 shows the voltage across the matched load. This simulation used a timestep equal to one-half of the Courant limit, 24.75 ps.

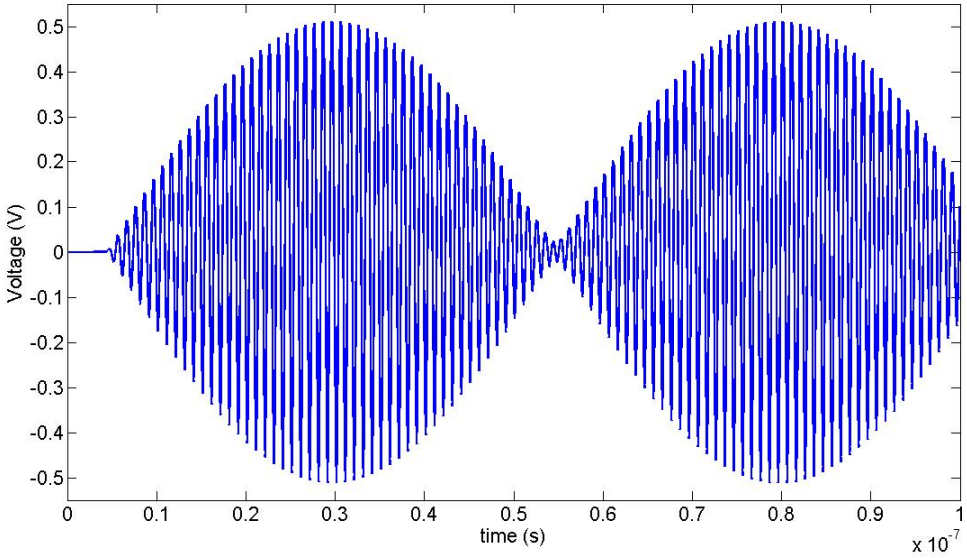

Figure 5.9: Voltage waveform appearing at the midpoint of the transmission line simulated using the univariate trapezoidal method.

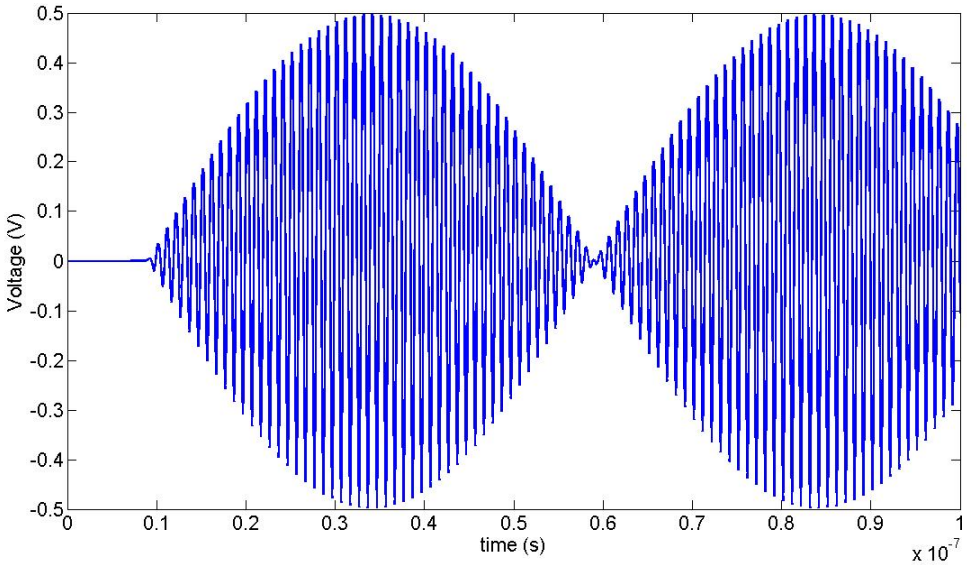

Figure 5.10: Voltage waveform appearing at the load of the transmission line simulated using the univariate trapezoidal method.

The advantage to using the TD-ENV method over the MFDTD method is most evident when the size of the problem becomes large. Because a smaller matrix system must be solved at each time point along the t_1-axis, the overall simulation time is reduced significantly with the TD-ENV method for larger problems. More importantly, however, the TD-ENV method allows for the solution of larger problems (e.g., longer transmission lines), in cases for which using the MFDTD method is not feasible. As the problem sizes get larger, the MFDTD will fail much sooner than the TD-ENV method because of memory constraints. In addition, the TD-ENV method provides the shortest simulation time. To highlight the point, Table 5.1 shows the time needed to simulate the transmission line example for each of the three simulation methodologies under consideration. The times listed in Table 5.1 are typical values of the time required to simulate the problem on a Toshiba laptop running Microsoft Windows XP.

Table 5.1: Time needed to simulate the transmission line example using each of the simulation methodologies under consideration.

	Univariate trapezoidal	MFDTD	TD-ENV
Simulation time (s)	15.453	25.328	2.984

Now, the TD-ENV method does not directly exploit the periodicity that may appear in the slowest time scale (for the case of quasi-periodic signals). Consequently, there seems to be slight dispersion in the early-time response, so there is some error in the capture of the delay, as evident from Figures 5.7 and 5.8. Because the periodicity of the slowest time scale is not directly enforced, the TD-ENV method takes some time to establish the true shape of the envelope function, and this is seen as a dispersion error in

the propagating waveforms. This effect can be ameliorated by increasing the sampling of the envelope signal. Generally, however, the true periodicity of the waveform is not seen until the second lobe of the multivariate signals, as evidenced by the figures.

An alternative approach to enabling the solution of larger problems via the MFDTD method is to decompose a long transmission line into several smaller lines. This relaxation-type method will facilitate the efficient solution of large problems using the MFDTD method via a decomposition approach similar to the one presented in Chapter 4.

5.5.2 Transmission line with periodically varying dielectric

Now consider the same circuit as shown in Figure 5.4, except with the shunt capacitances now varying sinusoidally in time around a center capacitance C_0,

$$C(t) = C_0 + C_1 \sin\left(2\pi f_C t + \varphi\right). \tag{5.15}$$

Obviously the amplitude of variation given by C_1 must be less than the magnitude of the center capacitance in order to maintain a positive value for the dielectric material of the line. In order to demonstrate that this type of periodic variation in the dielectric property of a transmission line does indeed result in a quasi-periodic behavior of the state variables in the resulting system, consider the discrete section of transmission line shown in Figure 5.11.

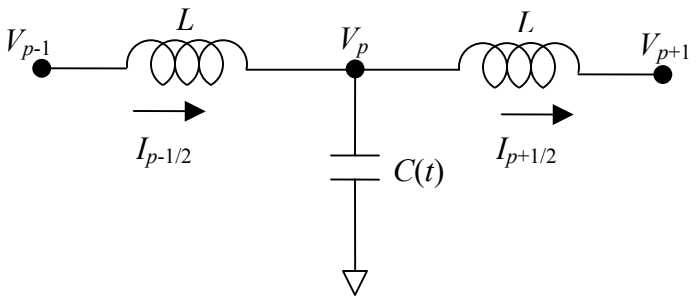

Figure 5.11: Section of a transmission line with time-varying capacitance.

Now, the section of transmission line shown in Figure 5.11 has been labeled with voltage and current variables staggered in space to mimic the discretization provided by a one-dimensional Yee's lattice. This spatial discretization is designated by the subscript in each variable. Based on this section of transmission line, the telegrapher's equations governing wave propagation can be derived as

$$V_p - V_{p+1} = L\frac{\partial I_{p+1/2}}{\partial t} \tag{5.16}$$

$$I_{p-1/2} - I_{p+1/2} = \frac{\partial\left(CV_p\right)}{\partial t} = \frac{\partial C}{\partial t}\cdot V_p + C\frac{\partial V_p}{\partial t}. \tag{5.17}$$

It is evident from Equation (5.17) that the consequence of a time-varying shunt capacitance in the transmission line is a conductance equal to the time derivative of the capacitance. Now, for the case of periodic or quasi-periodic input excitation to the transmission line and periodic variation in the capacitance, the form of Equation (5.17) shows that the resulting state variables will also be quasi-periodic, meaning that the MPDE formulations of this chapter are relevant simulation methodologies for this type of problem. Therefore, we can introduce multivariate formulations for each of the variables

in Equations (5.16) and (5.17). Assuming a single frequency sinusoidal source and a sinusoidally varying capacitance, we have

$$\hat{V}_p - \hat{V}_{p+1}\Big|_{\frac{(m,n)+(m,n-1)}{2}} = L\left(\frac{\hat{I}_{p+1/2}(m,n)-\hat{I}_{p+1/2}(m-1,n)}{\Delta t_1}+\frac{\hat{I}_{p+1/2}(m,n)-\hat{I}_{p+1/2}(m,n-1)}{\Delta t_2}\right) \tag{5.18}$$

$$\hat{I}_{p-1/2} - \hat{I}_{p+1/2}\Big|_{\frac{(m,n)+(m,n-1)}{2}} = \frac{\partial C}{\partial t}\cdot V_p + C\frac{\partial V_p}{\partial t}. \tag{5.19}$$

To illustrate the use of the TD-ENV simulation methodology for this type of problem, consider a transmission line of length equal to five wavelengths with a time-varying capacitance with characteristics $C_0 = \Delta z / C_{pul} v_p$, $C_1 = 0.1 \cdot C_0$, f_C = 1 GHz, and $\varphi = 0$. A sinusoidal source with frequency 10 MHz is used to excite the line. In calculating the impedance and propagation delay of the line, the variation in capacitance was actually ignored. As a result, there is expected to be a slight reflection at both the source and load ends of the line due to the impedance mismatch, although the level of mismatch is changing with time. For the envelope-modulated simulation, 30 points per period were used to capture the envelope function, while 15 points per period were used for the high-frequency oscillation of the variable capacitors.

The results of this simulation are shown in Figures 5.12 and 5.13. The results of the simulation using a standard univariate trapezoidal method with constant timestep equal to one half of the CFL limit are shown superimposed on the same figures. It is evident from the figures that the waveforms along this transmission line do display quasi-periodic or envelope-modulated behavior. Again, the TD-ENV provides a much more efficient means of simulating this type of problem while maintaining good accuracy.

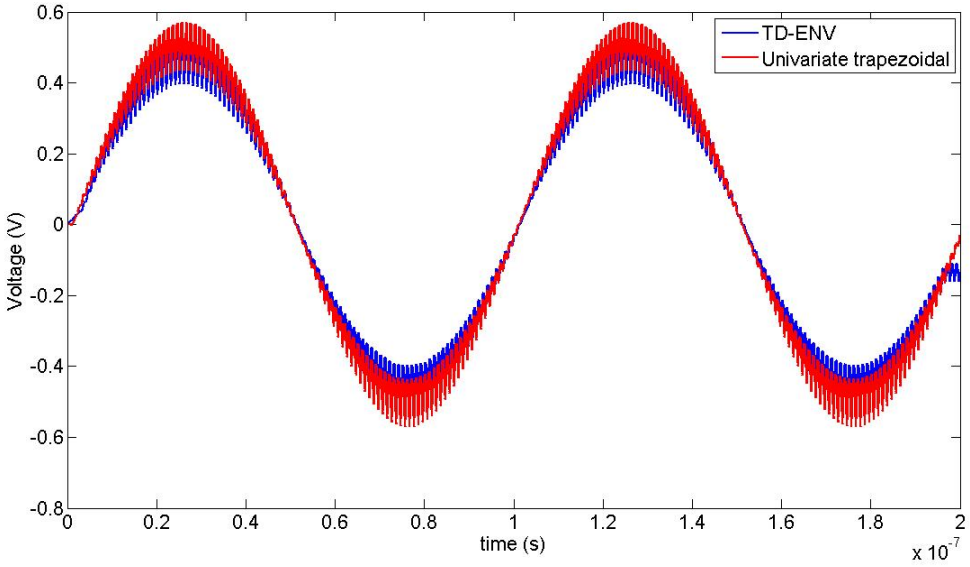

Figure 5.12: Voltage waveform appearing at the midpoint of the transmission line with periodically varying dielectric.

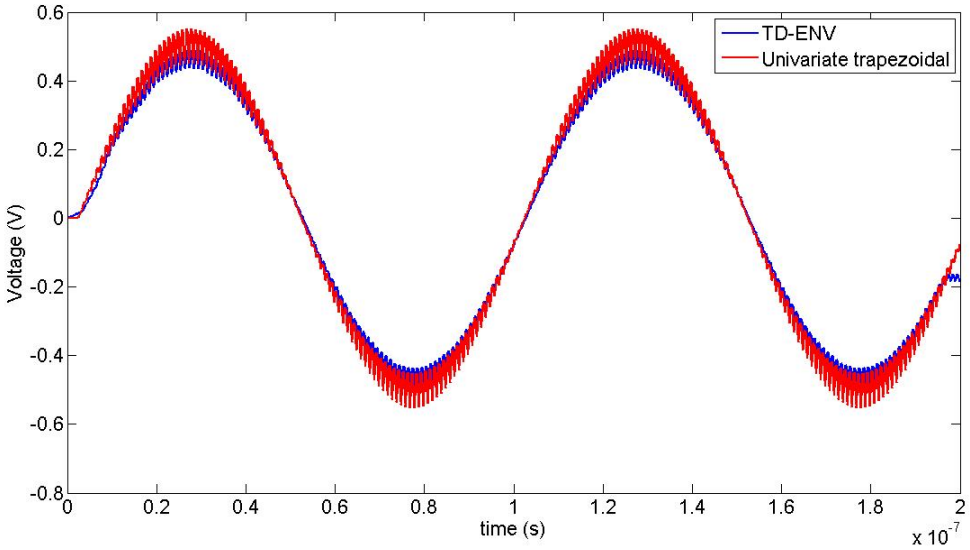

Figure 5.13: Voltage waveform appearing at the load of the transmission line with periodically varying dielectric.

It is evident from the figures that the waveforms found via the TD-ENV method exhibit more signal degradation than those found using a univariate trapezoidal method. However, the integrity of the frequency content seems intact. This difference between

the two simulation methodologies is attributed to the fact that the time variation of the per-unit-length capacitance in the line is updated more frequently in the univariate simulation because of the smaller timesteps. However, there is significant improvement in the run time involved by using the TD-ENV method. For this example, a 93% savings in simulation time was witnessed.

5.6 Comments and Conclusions

The methodology presented in this chapter illustrates an efficient means of capturing widely spaced periodically varying signals. While the multivariate form provides a compact representation for these types of signals, the true efficiency of the MFDTD solution process is nevertheless hindered by the fact that all time points are solved for at once. This means that if the size of the original circuit is *N*, then the size of the system that must be solved is $n_1 \cdot n_2 \cdots n_M \cdot N$. Clearly, this can quickly make problems prohibitively large, especially for the distributed, transmission line circuits that are of particular concern to us in this dissertation. Therefore, the true practical value of this methodology is contingent upon being able to find effective model order reduction techniques or other methods for simplifying the complexity of the resulting sparse linear system. In particular, a decomposition approach similar to the one introduced in Chapter 4 can be considered to improve the solution process with the MFDTD method.

The TD-ENV solution process eases the memory constraints of the MFDTD process by considering the most slowly varying signal as an envelope to the higher-frequency directions. As such, it has clearly established itself as the most efficient solution

methodology among the ones studied for the purpose of simulation involving quasi-periodic or envelope-modulated signals.

CHAPTER 6

CONCLUSION AND FUTURE WORK

6.1 Overview and Impact of Results

In this dissertation, three methodologies have been presented to enable the efficient, accurate simulation of hybrid electromagnetic/circuit systems. One of the main challenges in performing such hybrid simulations is in achieving a seamless interface between the distributed and lumped components, especially since the timestep used for the distributed components is often intrinsically limited by the CFL criterion because of the explicit time integration rule.

The first method proposed in this dissertation enabled a direct circuit representation of a distributed structure defined on a rectangular Yee's lattice. By identifying electric and magnetic field variables in the distributed structure with voltage and current unknowns in the circuit domain, standard SPICE-like circuit simulators can be utilized in the solution process. The advantage to this method over most existing methods for describing circuit representations of distributed structures is that the existing methods typically use a port-based description of the structure, thus losing the full-wave description that an electromagnetic solution normally provides. This method, on the other hand, uses a literal interpretation of the electromagnetic description in terms of circuit variables, thus keeping the nature of the full-wave solution process intact to the accuracy provided by the spatial discretization of the Yee's lattice.

The second method proposed in this dissertation was a decomposition method that enabled the simultaneous solution of both distributed and lumped components via FDTD and standard circuit numerical integration schemes using different timesteps for each component. Inspired by the substitution theorem from classical network theory as well as waveform relaxation methods from circuit analysis, the method used dependent sources to provide for the interaction between the various components. While somewhat similar in formulation to existing hybrid FDTD/circuit analysis methods, the primary achievement seen here is that the timestep used in the simulation of the lumped components is not limited by the CFL stability criterion, which governs the timestep used in the distributed components. While there are limitations on how far the timestep can be moved away from the CFL limit, this approach does nevertheless allow for a more efficient simulation process.

In order to further improve upon this method, the Crank-Nicolson scheme was introduced in the simulation of distributed, electromagnetic structures such as transmission lines. It was seen that the Crank-Nicolson method allows for an efficient simulation process with little dispersion and without the stability constraints of the standard FDTD method. However, when used in conjunction with the decomposition scheme, this solution methodology did display some spurious errors that are not well understood. Further investigation is required in this direction to improve the results.

The third and final method introduced here was the simulation of transmission line circuits using a multivariate PDE formulation of the circuit equations. This allows for a compact representation of signals displaying multirate behavior. Examples showed that such signals could be propagated down the transmission line circuit with an acceptable

level of numerical dispersion if a trapezoidal-type rule is used for the numerical integration. In addition, by considering the most slowly varying component of these multirate signals as an envelope to the higher-frequency components, the efficient simulation of large transmission line circuits was enabled, with considerable savings in simulation time over univariate approaches.

6.2 Future Work

Further efforts in the direction of the decomposition scheme of Chapter 4 include the implementation of more nonlinear devices within the SPICE-like framework, as well as the incorporation of more complicated distributed structures encapsulated in the SPICE paradigm via the simulation methodology of Chapter 3, to better demonstrate the capabilities of the proposed scheme. The introduction of nonlinear elements will, it is hoped, enable a deeper study of the phenomenon of passive intermodulation, which is garnering increasing interest in the RF community. Also, further study into the use of the Crank-Nicolson scheme in conjunction with the decomposition scheme is needed to better understand the current inadequacy of the method and present solutions.

Future work to be done in the direction of the multivariate PDE method includes combining the MFDTD method with the decomposition methods of Chapter 4. Finally, passive intermodulation noise arising from nonlinear elements can be studied in this context also.

REFERENCES

[1] J. K. White, "The multirate integration properties of waveform relaxation, with applications to circuit simulation and parallel computation," in *Electrical Engineering and Computer Science*. Berkeley, CA: University of California at Berkeley, Tech. Rep. UCB/ERL M85/90, 1985.

[2] T. L. Pillage, R. A. Rohrer, and C. Visweswariah, *Electronic Circuit and System Simulation Methods*. New York, NY: McGraw-Hill, 1994.

[3] J. Vlach and K. Singhal, *Computer Methods for Circuit Analysis and Design*, 2nd ed. New York, NY: Chapman & Hall, 1993.

[4] A. Taflove and S. C. Hagness, *Computational Electrodynamics: The Finite-Difference Time-Domain Method*, 3 ed. Norwood, MA: Artech House, 2005.

[5] K. S. Yee, "Numerical solution of initial boundary value problems involving Maxwell's equation in isotropic media," *IEEE Transactions on Antennas and Propagation*, vol. AP-14, no. 302-307, May 1966.

[6] C. A. Balanis, *Advanced Engineering Electromagnetics*. New York, NY: John Wiley & Sons, 1989.

[7] E. Yamashita, K. Atsuki, and T. Hirahata, "Microstrip dispersion in a wide-frequency band," *IEEE Transactions on Microwave Theory and Techniques*, vol. 29, no. 6, pp. 610-611, June 1981.

[8] H. Guckel, P. A. Brennan, and I. Palocz, "A parallel-plate waveguide approach to microminiaturized, planar transmission lines for integrated circuits," *IEEE Transactions on Microwave Theory and Techniques*, vol. 15, no. 8, pp. 468-476, August 1967.

[9] E. Hammerstad and O. Jensen, "Accurate models for microstrip computer-aided design," presented at IEEE Microwave Theory and Techniques Society International Symposium Digest, Washington, DC, 1980.

[10] U. S. Inan and A. S. Inan, *Engineering Electromagnetics*. Menlo Park, CA: Addison Wesley Longman, Inc., 1999.

[11] R. Courant, K. O. Friedrichs, and H. Lewy, "Uber die partiellen Differenzengleichungen der mathematischen Physik," *Mathematische Annalen*, vol. 100, no. 1, pp. 32-74, December 1928.

[12] J. P. Boyd, *Chebyshev and Fourier Spectral Methods*, 2nd ed. Mineola, NY: Dover, 2001.

[13] W. Sui, D. A. Christensen, and C. H. Durney, "Extending the two-dimensional FDTD method to hybrid electromagnetic systems with active and passive lumped elements," *IEEE Transactions on Microwave Theory and Techniques*, vol. 40, no. 4, pp. 724-730, April 1992.

[14] M. Piket-May, A. Taflove, and J. Baron, "FD-TD modeling of digital signal propagation in 3-D circuits with passive and active loads," *IEEE Transactions on Microwave Theory and Techniques*, vol. 42, no. 8, pp. 1514-1523, August 1994.

[15] P. Ciampolini, P. Mezzanotte, L. Roselli, and R. Sorrentino, "Accurate and efficient circuit simulation with lumped-element FDTD technique," *IEEE Transactions on Microwave Theory and Techniques*, vol. 44, no. 12-1, pp. 2207-2215, December 1996.

[16] V. A. Thomas, M. E. Jones, M. Piket-May, A. Taflove, and E. Harrigan, "The use of SPICE lumped circuits as sub-grid models for FDTD analysis," *IEEE Microwave and Guided Wave Letters*, vol. 4, no. 5, pp. 141-143, May 1994.

[17] C. Kuo, V. A. Thomas, S. T. Chew, B. Houshmand, and T. Itoh, "Small signal analysis of active circuits using FDTD algorithm," *IEEE Microwave and Guided Wave Letters*, vol. 5, no. 7, pp. 216-218, July 1995.

[18] A. Witzig, C. Schuster, P. Regli, and W. Fichtner, "Global modeling of microwave applications by combining the FDTD method and a general semiconductor device and circuit simulator," *IEEE Transactions on Microwave Theory and Techniques*, vol. 47, no. 6-2, pp. 919-928, June 1999.

[19] W. Sui, *Time-Domain Computer Analysis of Nonlinear Hybrid Systems*. Boca Raton, FL: CRC Press, 2002.

[20] K. Aygun, B. Fischer, J. Meng, B. Shanker, and E. Michielssen, "A fast hybrid field-circuit simulator for transient analysis of microwave circuits," *IEEE Transactions on Microwave Theory and Techniques*, vol. 52, no. 2, pp. 573-583, February 2004.

[21] C. Yang and V. Jandhyala, "Coupled circuit-electromagnetic simulation with time domain integral equations," presented at IEEE Antennas and Propagation Society International Symposium, Columbus, OH, 2003.

[22] V. Jandhyala, Y. Wong, D. Gope, and C. J. R. Shi, "A surface-based integral equation formulation for coupled electromagnetic and circuit simulation," *Microwave and Optical Technology Letters*, vol. 34, no. 2, pp. 103-106, July 2002.

[23] A. E. Yilmaz, J.-M. Jin, and E. Michielssen, "A TDIE-based asynchronous electromagnetic-circuit simulator," *IEEE Microwave and Wireless Components Letters*, vol. 16, no. 3, pp. 122-124, March 2006.

[24] R. D. Malucci, "High frequency considerations for multi-point contact interfaces," presented at 47th IEEE Holm Conference on Electrical Contacts, Montreal, Canada, 2001.

[25] J. D. Lavers and R. S. Timsit, "Constriction resistance at high spatial frequencies," *IEEE Transactions on Components and Packaging Technologies*, vol. 25, no. 3, pp. 446-452, September 2002.

[26] W. H. Higa, "Spurious signal generated by electron tunneling on large reflector antennas," *Proceedings of the IEEE*, vol. 63, no. 2, pp. 306-313, February 1975.

[27] A. D. Bond, C. S. Guenzer, and C. A. Carosella, "Intermodulation generation by electron tunneling through aluminum-oxide films," *Proceedings of the IEEE*, vol. 67, no. 12, pp. 1643-1653, December 1979.

[28] A. Ramachandran, A. Ramachandran, and A. C. Cangellaris, "SPICE-compatible stamps for semi-discrete approximations of Maxwell's equations," *International Journal of Numerical Modelling*, vol. 21, no. 4, pp. 265-277, July 2008.

[29] A. E. Ruehli and A. C. Cangellaris, "Progress in the methodologies for the electrical modeling of interconnects and electronic packages," *Proceedings of the IEEE*, vol. 89, no. 5, pp. 740-771, May 2001.

[30] M. S. Nakhla and J. Vlach, "A piecewise harmonic balance technique for determination of periodic response of nonlinear systems," *IEEE Transactions on Circuits and Systems*, vol. CAS-23, no. 2, pp. 85-91, February 1976.

[31] C. E. Christoffersen, M. B. Steer, and M. A. Summers, "Harmonic balance analysis for systems with circuit-field iterations," presented at IEEE Microwave Theory and Techniques Society Symposium, Baltimore, MD, 1998.

[32] E. Lelarasmee, A. E. Ruehli, and A. L. Sangiovanni-Vincentelli, "The waveform relaxation method for time-domain analysis of large scale integrated circuits," *IEEE Transactions on Computer-Aided Design of Integrated Circuits and Systems*, vol. CAD-1, no. 3, pp. 131-145, July 1982.

[33] A. R. Newton and A. L. Sangiovanni-Vincentelli, "Relaxation based electrical simulation," *IEEE Transactions on Computer-Aided Design of Integrated Circuits and Systems*, vol. CAD-3, no. 4, pp. 308-330, October 1984.

[34] M. C. Taylor and T. K. Sarkar, "WIPL-D model and simulation results for a 46 cm diameter impulse radiating antenna (IRA)," presented at IEEE Antennas and Propagation Society International Symposium, Washington, DC, 2005.

[35] A. Y. Woo and A. C. Cangellaris, "PRePFit: Passive rational approximation of a passive network transfer function from its real part," *International Journal of RF and Microwave Computer-Aided Engineering*, vol. 18, no. 3, pp. 209-218, March 2008.

[36] A. Y. Woo and A. C. Cangellaris, "Passive rational fitting of a driving-point impedance from its real part," presented at 10th IEEE Workshop on Signal Processing in Interconnects, Berlin, Germany, 2006.

[37] A. Y. Woo and A. C. Cangellaris, "Real-part sufficiency and its application to the rational function fitting of passive electromagnetic responses," presented at IEEE Microwave Theory and Techniques Society International Symposium, Honolulu, Hawaii, 2007.

[38] W. H. Press, S. A. Teukolsky, W. T. Vetterling, and B. P. Flannery, *Numerical Recipes: The Art of Scientific Computing*, 2nd ed. Cambridge, United Kingdom: Cambridge University Press, 1992.

[39] J. Roychowdhury, "Analyzing circuits with widely separated time scales using numerical PDE methods," *IEEE Transactions on Circuits and Systems - I: Fundamental Theory and Applications*, vol. 48, no. 5, pp. 578-594, May 2001.

[40] E. Ngoya and R. Larcheveque, "Envelop transient analysis: A new method for the transient and steady state analysis of microwave communication circuits and systems," presented at IEEE Microwave Theory and Techniques Society International Symposium, San Francisco, CA, 1996.

[41] M. Farkas, *Periodic Motions*. New York, NY: Springer-Verlag, 1994.

AUTHOR'S BIOGRAPHY

Anand Ramachandran received the B.S. in electrical and computer engineering from Duke University, Durham, NC, in December 2001 and the M.S. in electrical and computer engineering from the University of Illinois at Urbana-Champaign (UIUC) in May 2005. He was a Ph.D. candidate at UIUC from May 2005 to January 2009, focusing his research on applied and computational electromagnetics with an emphasis on hybrid electromagnetic and circuit solvers in the time domain.

Since February 2009, he has been with Northrop Grumman Electronic Systems, Baltimore, MD, where he has been working on the design of radar systems and components.